

國立交通大學

分子科學所

碩士論文

探究三甲基鋁在空氣中的自燃反應

Why Is Trimethylaluminum Hypergolic in the Air

研究生 唐欣瑜

指導教授 林明璋 院士

民國九十八年七月

探究三甲基鋁在空氣中的自燃反應

Why Is Trimethylaluminum Hypergolic in the Air

研究生：唐欣瑜

Student : Hsin-Yu Tang

指導教授：林明璋

Advisor : Ming-Chang Lin

國立交通大學

分子科學所

碩士論文

A Thesis

Submitted to Department of Applied Chemistry and Institute of Molecular Science

National Chiao Tung University

in partial Fulfillment of the Requirements

for the Degree of

Master

in

Applied Chemistry

July 2008

Hsinchu, Taiwan, Republic of China

中華民國九十八年八月

摘要

“為什麼三甲基鋁(Trimethylaluminum)會在空氣中自燃?是個非常有趣且值得深入探討的現象。三甲基鋁與空氣混合自燃爆炸，此現象伴隨著熱能的釋放亦或是自由基(Radical)的產生。這些由初始反應生成的自由基可以很快的再與空氣中其他分子再次碰撞，產生連鎖反應釋放出更多的熱能，也因此三甲基鋁常被用來作為初始火箭的燃料。我們猜測此自燃反應可能是三甲基鋁與空氣中的氣體：水分子及氧氣產生作用。為了驗證這個想法，在本研究中，我們利用 Gaussian 氣相反應模擬軟體，計算水分子或是氧氣與三甲基鋁之反應，找出可能的反應路徑及反應中可能存在的中間產物和最終物。

從計算的結果得知，三甲基鋁無法直接跟氧氣形成穩定的中間產物。反之，此反應直接跨越一過渡能階，使得三甲基鋁可與氧氣鍵結產生 $(\text{CH}_3)_3\text{AlO}_2$ 。此反應的能障僅約 10 千卡，可被克服使反應持續進行。在下一個反應步驟中，經由給與少許能焓，一個甲基可直接從 $(\text{CH}_3)_3\text{AlO}_2$ 分子中被釋放出來。

另外，三甲基鋁可與水形成相對穩定的中間產物 $((\text{CH}_3)_3\text{AlOH}_2)$ ，並釋放出每莫耳約 17 千卡的能量。此中間產物更只需要跨越一極小的能障便可進一步反應形成甲烷及 $(\text{CH}_3)_2\text{AlOH}$ ，並釋放出每莫耳約 35 千卡的能量。 $(\text{CH}_3)_2\text{AlOH}$ 亦可能再次產生甲烷，但必須克服每莫耳約 30 千卡能障。雖然相對高於形成第一個甲烷的能量，但是反應仍有可能發生。反應過程中產生的甲烷，亦可參與後續

的燃燒反應。

三甲基鋁亦有可能熱分解成二甲基鋁(Dimethylaluminum)。計算結果顯示，讓水與二甲基鋁結合成 $(\text{CH}_3)_2\text{AlOH}_2$ 伴隨著每莫耳約 14 千卡的能量被釋放。與三甲基鋁跟水反應的過程類似，在經過每莫耳 3 千卡的過渡態，釋放出第一個甲烷，能量相對於反應物下降了每莫耳 33 千卡，並生成 CH_3AlOH 。再經過另一每莫耳 10 千卡的過渡態， CH_3AlOH 可分解出第二個甲烷及氧化鋁自由基(AlO)。此反應之產物相對能量僅僅高於反應物每莫耳 2.8 千卡。

若是將氧氣與三甲基鋁撞碰，氧氣不易直接與三甲基鋁鍵結不利於反應的進行。故先將水分子與三甲基鋁鍵結，利用水分子與氧氣形成物理快吸附，再讓氧氣進一步氧化三甲基鋁。但必須經過一每莫耳吸熱約 24 千卡的過渡態，氧氣才可直接與鋁原子鍵結並釋放出一個甲基，甲基可再與空氣中氧氣分子反應。

三甲基鋁亦可自發性的生成雙分子三甲基鋁。實驗值顯示，雙分子的鍵結能大約為 20 千卡。我們由比較實驗和計算結果之鍵結能，可選擇出較適當的計算方法來計算雙分子三甲基鋁與氧氣的反應。

延續在三甲基鋁自發性吸附成雙分子三甲基鋁的初步結果，雙分子三甲基鋁接著可與氧氣反應。雙分子三甲基鋁僅需與一個氧氣分子反應，就可釋放出兩個甲基。且反應不僅伴隨大量的能量釋放，反應中唯一的能障比反應物的相對能量低約 2 千卡，此低能障幾乎無法對反應造成阻礙。故在這五種反應中，我們認為三甲基鋁在空氣中自燃最主要的反應路徑應為雙分子三甲基鋁與氧氣反應。

我們利用 Gaussian 氣相量子模擬軟體，對三甲基鋁與水分子和氧氣及雙分子三甲基鋁與氧氣之反應進行理論計算，發現這些反應均伴隨大量能量的釋放亦或是自由基的產生而利於連鎖反應，這樣的結果成功地說明了三甲基鋁在空氣中可自燃爆炸的現象。因此，此模擬計算可能亦適用於其他類似的爆炸或自燃性反應。



ABSTRACT

“Why is trimethylaluminum (TMAI, $(\text{CH}_3)_3\text{Al}$) hypergolic in the air?” is a very interesting question which is worth studying. To unveil the hypergolic phenomenon, the Gaussian code (a computational chemistry software) was applied to simulate the reactions of TMAI with oxygen and/or water molecules. Possible paths of reactions and the structures and energies of the reactants, intermediates, and products in the reactions were determined by ab initio molecular orbital calculations.

The results of calculations show that, a transition state with about 10 kcal/mol barrier has to be overcome in the process of TMAI binding with an O_2 molecule, instead of directly forming a stable intermediate at the initial step. After passing through the transition state, $(\text{CH}_3)_3\text{AlO}_2$ molecule can be formed by releasing one of the methyls from $(\text{CH}_3)_3\text{AlO}_2$ with a small activation barrier.

The calculational results show that TMAI can bind with a water molecule forming a stable complex, $(\text{CH}_3)_3\text{AlOH}_2$, with 17 kcal/mol binding energy. By overcoming across a small barrier (0.13 kcal/mol lower than the energy of reactants), one methane is released to form a stable product, $(\text{CH}_3)_2\text{AlOH}$, dimethylaluminum hydroxide, which may decompose to give a second methane molecule, but it has to overcome an energy barrier of 30 kcal/mol.

Another possible path, in which dimethylaluminum (DMAI, $(\text{CH}_3)_2\text{Al}$), formed by dissociating a methyl from TMAI, can react with another water molecule much more readily. The final products are two methane molecule and AlO radical. The reaction is endothermic by only about 2.8 kcal/mol.

Because of the co-existence of O_2 and H_2O molecules in the air, we have also investigated the termolecular reaction of TMAI with O_2 and H_2O molecule. Although O_2 molecule was formed to form a van der Waals complex with the TMAI: OH_2 intermediate, no significant lowering of the CH_3 production barrier was noted.

The monomers of TMAI can spontaneously associate to form a TMAI dimer. The association energy was experimentally determined to be about 20 kcal/mol, which was found to be consistent with the value, 21.59 kcal/mol, 18.21 kcal/mol and 16.79 kcal/mol predicted by G3B3, MP2, and DFT by VASP respectively.

In the reaction of dimer-TMAI with O_2 , two CH_3 radicals can be produced with a large amount of energy released. At the DFT level of theory, the largest energy barrier in the whole complex reaction was formed to be lower than the reactants by about 2 kcal/mol, suggesting that the reaction can occur readily at low temperature. This reaction is therefore considered to be the major path to

form radicals when TMAI contacts with air.

By theoretical simulations, we found that the reactions of TMAI with water, and oxygen molecules are highly exothermic and in the case of O_2 reaction CH_3 radicals can be produced. The results are consistent with the hypergolic property of TMAI and thus may be applied to other metal alkyl reactions.



Acknowledgement

論文寫到了這一頁，才真的驚覺將要與大家分離了。回憶起兩年前剛進實驗室的時候，我被分配給大大肚子的 AD 在燃料電池組，後來被阿福學長的實驗習慣嚇到跳到理論組，在教授的鼓勵下，跟賴科科一起傻傻的修了畢生以來修過最無厘頭的“量子化學”，一起連續七、八小時的馬拉松考試，總算是大家都過通了。去年的暑假，又有一群天真的朋友加入了我們實驗室。大家一起修老師的課，一起挨過每個難熬的星期五早晨時光，還有聽冠霖報告今天老師又刷新連續 181 分鐘不下課紀錄。或許就在那時建立起我們有福不分享，有難必同當的情操。

兩年在實驗室碩士的時間，實在不短，但真的就這樣無聲無息的流過。只是我的腦袋裡已裝了滿滿跟大家一起同甘共苦的回憶。感謝林明璋老師在這兩年間對我的照顧與諄諄教誨。感謝 Dr. Hue 在我即將畢業的日子裡，與我一而再，再而三的檢查論文的計算結果，幫我完成了很多不可能的任務。感謝陳博在我還是小碩一時，很有耐心的教我怎麼跑 Gaussian。感謝雯妃學姐教我跑 VASP，且總是不厭其煩的聆聽我許多許多的問題，不論是學業上或是生活上。感謝 AD 不時露出他的大肚腩並分享他與小錚最新動向的八卦取悅大家。感謝科科時而語出驚人的種種賴氏謬論。感謝雯傑在 TFT 上的教導。感謝志翰成為我修習 TFT 最好的對象；感謝冠霖三不五時就會丟個“輕鬆一下”的 youtube 影片；這些都讓我在忙碌的研究中能獲得些許喘息。感謝 D 大與老王不經意的讓六人行的戲碼在實驗室上演，為我枯燥的研究生生活添增不少樂趣。感謝帥坤在這一路上的陪伴與鼓

勵，還在我口試時幫我打點口試的細節，讓我可以專心的準備口試。感謝所有實驗室同仁，是你們讓我能擁有這些寶貴的回憶，開心、滿足地離開這間充滿回憶的地方，我一定不會忘記你們一張張可愛的臉。天下沒有不散的筵席，祝大家都一路順風，期待我們再相聚的時候。



TABLE OF CONTENTS

摘要(Chinese Abstract)	i
Abstract.....	iv
Acknowledgement.....	vii
Table of Contents	ix
List of Figures	xi
List of Tables	xii
Chapter 1. Introduction	1
Chapter 2. Computational Method	5
2.1 Fundamentals of quantum chemistry	6
2.2 Hartree-Fock theory	9
2.3 Basis function.....	12
2.4 Density functional theory.....	14
2.5 Optimization of geometry and computational frequency	16
Chapter 3. Results and Discussion	19
3.1 Reactions of Trimethylaluminum (CH ₃) ₃ Al and O ₂	19
3.2 Reactions of Trimethylaluminum (CH ₃) ₃ Al and water	27
3.3 Reactions of Dimethylaluminum (CH ₃) ₂ Al and water	35

3.4 Reaction of Trimethylaluminum, O ₂ and H ₂ O	41
3.5 Associating process of TMAI	47
3.6 Reaction of two Trimethylaluminums and O ₂	50
Chapter 4. Conclusion	60
References	64



LIST OF FIGURES

Figure 1.1.1 Optimized geometry of TMAI computed by B3LYP	3
Figure 2.5.1 Potential energy surface (PES) of a reaction	16
Figure 3.1.1 Optimized geometries of species in the TMAI + O ₂ reaction	20
Figure 3.1.2 Potential energy surface of the TMAI + O ₂ reaction	21
Figure 3.2.1 Optimized geometries of species in the TMAI + H ₂ O reaction ..	28
Figure 3.2.2 Potential energy surface of the TMAI + H ₂ O reaction.....	29
Figure 3.3.1 Optimized geometries of species in the DMAI + H ₂ O reaction ..	36
Figure 3.3.2 Potential energy surface of the DMAI + H ₂ O reaction	37
Figure 3.4.1 Optimized geometries of species in the TMAI + O ₂ + H ₂ O reaction	42
Figure 3.4.2 Potential energy surface of the TMAI + O ₂ + H ₂ O reaction.....	43
Figure 3.5.1 Association reaction of TMAI.....	58
Figure 3.6.1 Optimized geometries of species by B3LYP in the 2TMAI + O ₂ reaction	51
Figure 3.6.2 Potential energy surface of the 2TMAI + O ₂ reaction by B3LYP	52
Figure 3.6.3 Optimized geometries of species by VASP in the 2TMAI + O ₂ reaction	56
Figure 3.6.4 Potential energy surface of the 2TMAI + O ₂ reaction by VASP	57

LIST OF TABLES

Table 3.1.1 Geometrical details of all species in the TMAI + O ₂ reaction (Å).22	
Table 3.1.2 Species relative energy in the TMAI + O ₂ reaction (kcal/mol).....22	
Table 3.2.1 Geometrical details of all species in the TMAI + H ₂ O reaction (Å)30	
Table 3.2.2 Species relative energy in the TMAI + H ₂ O reaction (kcal/mol) ..30	
Table 3.3.1 Geometrical details of all species in the DMAI + H ₂ O reaction (Å)	
.....38	
Table 3.3.2 Species relative energy in the DMAI + H ₂ O reaction (kcal/mol)..38	
Table 3.4.1 Geometrical details of species in the TMAI + O ₂ + H ₂ O reaction (Å)	
.....44	
Table 3.4.2 Species relative energy in the TMAI + O ₂ + H ₂ O reaction (kcal/mol)	
.....44	
Table 3.5.1 TMAI association energies obtained by different methods.....49	
Table 3.6.1 Geometrical details of species in the dimer-TMAI + O ₂ reaction by B3LYP (Å)	53
Table 3.6.2 Geometrical details of species in the dimer-TMAI + O ₂ reaction by VASP (Å).....	58

1. Introduction

Ever since mankind first saw birds soaring through the sky, they dreamed to fly. The ancient Greeks and Romans pictured many of their gods with winged feet, and imagined various kinds of mythological winged animals. About 100 BC a Greek inventor known as Hero of Alexandria came up with a new invention that depended more on the mechanical interaction of heat and water. He invented a rocket-like device called an aeolipile. Steam was used for propulsion to rotate this device. In 1232 AD Chinese used rockets against the Mongols. Early Chinese rockets were used in warfare and celebrations. In fact, the origin of the rocket is shown simply in these Chinese characters (火箭). They stand for both "rocket" and "fire arrow." During 18th and 19th centuries, rockets were used only as weapons around the world. In the 19th century, rocket enthusiasts and inventors began to appear worldwide. By 1870, American and British inventors found different ways to use rockets. For example, the Congreve rocket was capable of carrying a line over 1000 feet to a stranded ship. In 1914, an estimated 1,000 lives were saved by this technique. In the 20th century, the rockets were designed to place manned or unmanned space capsules in orbiting flights. During 1971 and 1972, A Lunar

Roving Vehicle was used on each of the last three Apollo missions and the crews were permit to travel several miles from lunar landing sites.

Today's rockets are remarkable accumulations of human ingenuity. To make further improvement in the rocketry, it is very important to choose appropriate propellants. All the power of projecting the rocket comes from the fuel, thus the performance of the rocket is really correlative with what kind of fuel chosen. A great deal of propellant needs to be carried to the space, so its components must be light, small-volume and convenient for transportation.

When combustion starts, it reacts as quickly that the energy can be released in a very short time to push the projectile. There are three main types of propellants: solid, liquid, and hybrid. Liquid propellants are used commonly, because they are cheaper than others. And for another reason, liquid-fuelled rockets have better specific impulse than solid rockets and are capable of being throttled, shut down, and restarted. The first liquid-fuelled rocket, launched by Robert Goddard on March 16, 1926, used gasoline and liquid oxygen. The common liquid propellant combinations used today include liquid oxygen and liquid hydrogen, nitrogen tetroxide (N_2O_4) and hydrazine (N_2H_4), etc. Some light metal compounds (e.g., lithium, magnesium, and aluminum compounds etc.) react with oxygen and produce tremendous energy,

especially for trimethylaluminum (TMAI). It is hypergolic in air, and bursts in water. The major goal of this research is to study how it happens.

The structure of TMAI should be introduced here before discussing the details of this research. The geometry of TMAI is shown in Figure 1.1.1. and its chemical formula of TMAI is $\text{Al}(\text{CH}_3)_3$. It is formed by one aluminum binding with three methyls and has a planar structure. The bond length of Al-C is about 1.97 Å with low-rotational energy barriers for the methyl groups and the angle of C-Al-C is about 120° . In this research TMAI is used to react with molecules which exist in the air such as oxygen and water. Our strategy is to search for elementary reactions in which a large amount of energy is released or reactive radical products such as CH_3 are generated to initiate a chain process[1].

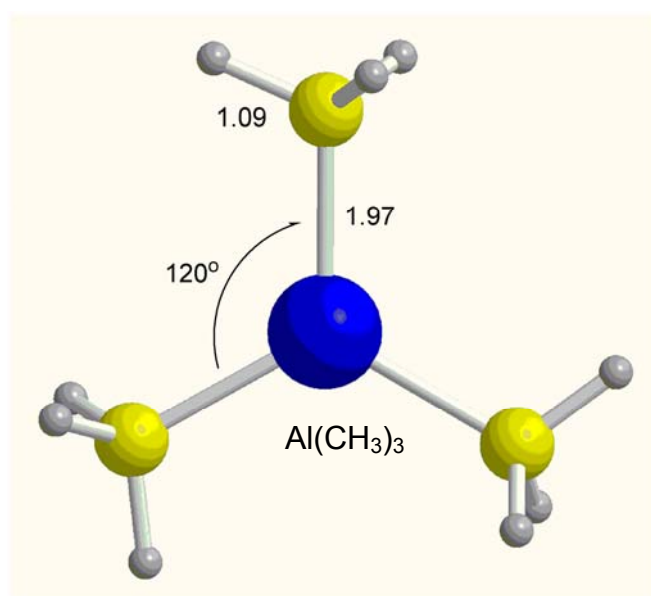


Figure 1.1.1 Optimized geometry of TMAI derived by B3LYP/[6-31+G(d,p)] (Å)

The following reactions have been investigated systematically: TMAI + O₂,
TMAI + H₂O, DMAI + H₂O, TMAI + O₂ + H₂O and 2TMAI + O₂.



2. Computational method

In this chapter, some concepts of the quantum mechanics and computational methods are reviewed briefly, for example, the Schrödinger equation, Hartree-Fock theory, basis function, and density functional theory. The Gaussian 03 program is applied in this research and all the computational works were carried out with the computer cluster, Spark, in the College of Science, NCTU.



2.1 Fundamentals of quantum chemistry

The fundamentals of the quantum mechanics are brought about by the great scientist, Erwin Schrödinger; the equation which describes how the quantum state of a physical system changes in time was named after him.

$$\hat{H}\psi = \varepsilon\psi \quad (2.1.1)$$

For a general case, there is usually more than one particle in the system. Thus this equation could be rewritten as follow for particle i ,

$$\hat{H}\psi_i = \varepsilon\psi_i \quad (2.1.2)$$

where \hat{H} is the Hamiltonian operator. It is generally written as

$$\begin{aligned} \hat{H} &= \hat{T}_N + \hat{T}_e + \hat{V}_{NN} + \hat{V}_{ee} + \hat{V}_{Ne} \\ &= \sum_N -\frac{\vec{\nabla}_N^2}{2m_N} + \sum_e -\frac{\vec{\nabla}_e^2}{2m_e} + \sum_N \sum_{N'(N < N')} \frac{Z_N Z_{N'}}{|\vec{r}_N - \vec{r}_{N'}|} \\ &\quad + \sum_e \sum_{e'(e < e')} \frac{1}{|\vec{r}_e - \vec{r}_{e'}|} - \sum_N \sum_e \frac{Z_N}{|\vec{r}_N - \vec{r}_e|} \end{aligned} \quad (2.1.3)$$

where \hat{T}_N is the kinetic energy of nuclei, \hat{T}_e the kinetic energy of electrons, \hat{V}_{NN} the coulomb repulsion potential energy between electrons, \hat{V}_{ee} the coulomb repulsion potential energy between nuclei, and \hat{V}_{Ne} the coulomb attracting potential energy between electrons and nuclei.

In equation (2.1.1), ψ is called a wavefunction. It is used to describe the wave-like behavior of particles. The other parameter in equation (2.1.1), \hat{H} , is a linear operator acting on the wavefunction ψ to get the total potential

energy of the system. The wavefunction, ψ , is the eigenfunction of \hat{H} , and ε is the eigenvalue of \hat{H} .

It is impossible to solve exactly the Schrödinger equation for a system greater than two particles. To solve this complicated equation, it must be simplified. Born-Oppenheimer approximation is later applied to multi-particle system. The main ideal of this approximation is that although the wavefunction behavior including nucleus and electrons, there is an enormous mass difference between nucleus and electron about 1836 times, so nucleus could be thought as an immobile body in the electron motion process. According to Born-Oppenheimer approximation, the original wavefunction, equation (2.1.3), could be rewritten as the product of the nucleus and electron wavefunction.

$$\Psi_{tot} = \psi_N(\vec{r}_N) \psi_e(\vec{r}_N, \vec{r}_e) \quad (2.1.4)$$

The Hamiltonian, \hat{H} , could be substituted by the Hamiltonian of nucleus, \hat{H}_N , and the electron, \hat{H}_e .

$$\hat{H}_{tot} = [\hat{T}_N + \hat{V}_{NN}] + [\hat{T}_e + \hat{V}_{ee} + \hat{V}_{Ne}] = \hat{H}_N + \hat{H}_e \quad (2.1.5)$$

Equation (2.1.1) could be written as follow:

$$\hat{H}_{tot} \Psi_{tot}(\vec{r}_N, \vec{r}_e) = (\hat{H}_N + \hat{H}_e) \Psi_{tot}(\vec{r}_N, \vec{r}_e) \quad (2.1.6)$$

After rewriting equation (2.1.4), the original Schrödinger equation could be separated into two partial differential equations, and find the solution

individually.

$$\hat{H}_N \psi_N = \varepsilon_N \psi_N \quad (2.1.7)$$

$$\hat{H}_e \psi_e = \varepsilon_e \psi_e \quad (2.1.8)$$

where \hat{H}_e become

$$\hat{H}_e = \sum_{i=1}^m \hat{h}(\vec{r}_i) + \sum_{i=1}^{2m-1} \sum_{j=i+1}^{2m} \hat{g}(\vec{r}_i, \vec{r}_j) \quad (2.1.9)$$

with

$$\hat{h}(\vec{r}_i) = -\frac{\hbar^2}{8\pi^2 m_e} \nabla_i^2 - \frac{e^2}{4\pi\epsilon_0} \sum_{\alpha=1}^N \frac{Z_\alpha}{R_{\alpha i}} \quad (2.1.10)$$

$$\hat{g}(\vec{r}_i, \vec{r}_j) = \frac{e^2}{4\pi\epsilon_0} \frac{1}{r_{ij}} \quad (2.1.11)$$

Applying equation (2.1.4) to equation (2.1.1)

$$\left(\hat{H}_N + \hat{H}_e \right) \psi_N \psi_e = \varepsilon_{tot} \psi_N \psi_e \quad (2.1.12)$$

and dividing equation (2.1.12) by $\psi_N \psi_e$ at the both side

$$\frac{1}{\psi_N \psi_e} \left(\hat{H}_N + \hat{H}_e \right) \psi_N \psi_e = \varepsilon_{tot} \quad (2.1.13)$$

Where \hat{H}_N and ψ_N are dependent on the position of the nucleus, and \hat{H}_e

and ψ_e are dependent on both of the nucleus and the electron.

2.2 Hartree-Fock theory

In the Born-Oppenheimer approximation, there is still some problem in solving the Schrödinger equations of electrons, equation (2.1.8). To find a reasonable solution according to Hartree-Fock theory[2], the total wavefunction of electrons is written as a product of the wavefunction of each electron. Because the electron is Fermion, in quantum mechanics, a Slater determinant is an expression which describes the wavefunction of a multi-fermionic system. For a molecule with m full orbitals:

$$\psi_e = (r_1, s_1, r_2, s_2, r_3, s_3, \dots, r_m, s_m) = \begin{vmatrix} \psi_A(r_1)\alpha(s_1) & \psi_A(r_1)\beta(s_1) & \psi_B(r_1)\alpha(s_1) & \dots & \psi_{M/2}(r_1)\beta(s_1) \\ \psi_A(r_2)\alpha(s_2) & \psi_A(r_2)\beta(s_2) & \psi_B(r_2)\alpha(s_2) & \dots & \psi_{M/2}(r_2)\beta(s_2) \\ \psi_A(r_3)\alpha(s_3) & \psi_A(r_3)\beta(s_3) & \psi_B(r_3)\alpha(s_3) & \dots & \psi_{M/2}(r_3)\beta(s_3) \\ \dots & \dots & \dots & \dots & \dots \\ \psi_A(r_m)\alpha(s_m) & \psi_A(r_m)\beta(s_m) & \psi_B(r_m)\alpha(s_m) & \dots & \psi_{M/2}(r_m)\beta(s_m) \end{vmatrix} \quad (2.2.1)$$

Where r is the position of electron, s is the spin of electron, and m is the orbital electron. This formula satisfies anti-symmetry requirements and subsequently the Pauli Exclusion principle by changing sign upon exchange of fermions.

Equation (2.2.1) is applied to (2.1.8), and mathematical method and undetermined Lagrange multiplier is used to work out the Hartree-Fock equation (2.2.2).

$$\hat{H}_i^F \psi_i = \varepsilon_i \psi_i \quad (2.2.2)$$

Where $\hat{H}_i^F = \hat{h}(\vec{r}_i) + V_{HF}$ is called Fock operator, the definition of $\hat{h}(\vec{r}_i)$ is shown in equation (2.1.10), and V_{HF} is the Hartree-Fock potential energy.

$$V_{HF}(\vec{r}_1) = \sum_i^{2m} (\hat{J}_i(\vec{r}_1) - \hat{K}_i(\vec{r}_1)) \quad (2.2.3)$$

Where $\hat{J}_i(\vec{r}_1)$ is the Coulomb operator,

$$\hat{J}_i(\vec{r}_1) = \int |\psi_i(\vec{r}_2)|^2 \frac{1}{r_{12}} d\vec{r}_2 \quad (2.2.4)$$

Where $\hat{K}_i(\vec{r}_1)$ is the exchange operator,

$$\hat{K}_i(\vec{r}_1)\psi_j(\vec{r}_1) = \int |\psi_i^*(\vec{r}_2)|^2 \frac{1}{r_{12}} \psi_j(\vec{r}_2) d\vec{r}_2 \psi_i(\vec{r}_1) \quad (2.2.5)$$

The calculus of variations, a field of mathematics, is used to find the eigenvalue of Hamiltonian (\hat{H}_i^F) in equation (2.2.2). The wavefunction of the molecular orbitals are thus expressed as linear combinations of basis functions, and the basis functions are wavefunction of atomic orbitals.

$$\psi_i = \sum_s^b c_{si} \chi_s \quad (2.2.6)$$

Applying this equation to (2.2.2),

$$\sum_s c_{si} \hat{H}_i^F \chi_s = \varepsilon_i \sum_s c_{si} \chi_s \quad (2.2.7)$$

The χ_r is multiplied on both sides of the equal. Equation (2.2.8) was obtained, and called Hartree-Fock-Roothaan equation.

$$\sum_{s=1}^b c_{si} (F_{rs} - \varepsilon_i S_{rs}) = 0, \quad r = 1, 2, \dots, b \quad (2.2.8)$$

$$F_{rs} \equiv \langle \chi_r | \hat{H}_i^* | \chi_s \rangle, \quad S_{rs} \equiv \langle \chi_r | \chi_s \rangle$$

To solve equation (2.2.8) with non-zero solutions, the determinant ($F_{rs} - \varepsilon_i S_{rs}$)

must be zero, i.e.,

$$\det(F_{rs} - \varepsilon_i S_{rs}) = 0 \quad (2.2.9)$$

To solve equation (2.2.9), the initial guess of electron orbital wavefunction must be given, then it is used to solve the eigenvalue, ε_i . This procedure is repeated until the difference of energy, ε_i , between the last two times is small than a limit given. This method is called self-consistent field, SCF.

Although the computational process is significantly simplified by using the Hartree-Fock method, computationally, there is still great deal of integral calculation to be made for a large system, especially for the integration of two-electron terms. Some Semi-empirical methods of computing the integration of two-electron terms are used to save time and to improve the computed efficiency for prediction of a large molecular system. In these methods, there are some parameters or neglected terms used based on experimental data to perform quantum calculations for a large system; for example, AM1[3] and PM3[4], etc. The electronic behavior in molecule could be described by these methods. For example, ZINDO[5] method is useful in simulating the spectrum of an organic molecule.

2.3 Basis function

If a realistic wavefunction is applied to equation (2.2.7), the mathematics would be too hard to be worked out and time consuming. This is the reason why the basis function is chosen to solve to equation (2.2.7).

Over the past decades, so much effort has been concentrated on using a special set of mathematic forms to represent the total wavefunction by changing the parameters in the set of mathematic forms. The Slater type basis function[6, 7] was developed first and applied in hydrogen-like atomic systems. Because this basis function is an exponential function, in the application of Hartree-Fock, the integration of exponential functions is truly complicated to solve.

To utilize Several Gaussian functions to represent the Slater type wavefunction was brought forth by John A. Pople, and co-works. The most important property of the Gaussian function is that it has an integrated form, and this property is advantageous to proceed computationally. This modified basis function is called an STOs/nG basis function.

This kind of wavefunctions then has been further developed into more flexible form, STOs/ $k-nlm$ G[8], where k mean the number of electron

wavefunctions in the center with fixed coefficient between the functions, n mean the number of the first set of Gaussian functions of electron wavefunction with fixed coefficient between the functions as well, and l and m are the number of the second and third set of Gaussian functions of electron wavefunctions, serially, and the parameter, n , l and m , are independent of each other. Every basis function with fixed coefficient could be thought as another set of constructed basis functions.

To make the basis function more flexible, the polarization function[9] is applied to the original basis function by J. B. Collin, et al. The higher level atomic orbital function is written into the basis functions to deal with the action of polarized electrons which is far from the nucleus.

There is the general writing for example, 6-31G* or 6-31G(d), where the asterisk or (d) denotes that a wavefunction of empty d orbital is added to the every heavy atom, and 6-31G** or 6-31G(d,p), where the two asterisks or (d,p) mean that not only the wavefunction of empty d orbital is added to heavy atoms but also an empty p orbital wavefunction is added to hydrogen.

In the case of the distribution of electron is extended, the diffuse function[10] is written into the basis function also. It means that another radial space is given to the atom to let the electron occupy. The general form is used

plus sign, +, for example, 6-31+G(d).

2.4 Density functional theory

Density functional theory (DFT) was presented to the public in 1964 by Hohenberg-Kohn. It is also called Hohenberg-Kohn theory[11], and could be simply explained by two key points as following:

1. From the quantum mechanics, the ground state energy is the function of the wavefunction as following,

$$E\left[\psi\left(\vec{r}_1, \vec{r}_2, \vec{r}_3, \dots, \vec{r}_N\right)\right] \quad (2.4.1)$$

According to DFT, the energy of the ground state is the functional of the electron density, and it could be rewritten as following,

$$E_{G.S.}\left[\psi\left(\vec{r}_1, \vec{r}_2, \vec{r}_3, \dots, \vec{r}_N\right)\right] \rightarrow E_{G.S.}\left[\rho\left(\vec{r}\right)\right] \quad (2.4.2)$$

Where

$$\rho\left(\vec{r}\right) = \sum_i \left|\psi_i\left(\vec{r}\right)\right|^2 \quad (2.4.3)$$

2. The variational principle is satisfied by energy functional of the ground state,

$E_{G.S.}\left[\rho\left(\vec{r}\right)\right]$; in other words, it must lead to

$$E_{G.S.}\left[\rho\left(\vec{r}\right)\right] \geq E_{G.S.}\left[\rho_{G.S.}\left(\vec{r}\right)\right] \quad (2.4.4)$$

According to these two points, the energy functional of the ground state could

be written as following,

$$E[\rho(r)] = T_s[\rho(r)] + V_{xc}[\rho(r)] + V_{ee}[\rho(r)] + V_{ext}[\rho(r)] \quad (2.4.5)$$

Kohn and Sham later solved equation (2.4.5) furthermore, then got the following equation,

$$-\frac{1}{2}\nabla^2\psi_i(\vec{r}) + V_{ext}(\vec{r})\psi_i(\vec{r}) + V_{ee}(\vec{r})\psi_i(\vec{r}) + V_{xc}(\vec{r})\psi_i(\vec{r}) = \lambda_i\psi_i(\vec{r}) \quad (2.4.6)$$

Where λ_i is the eigenvalue of equation (2.4.6) and it represent the energy of i orbital. The equation (2.4.6) is the well-known Kohn-Sham equation. The potential energy terms could be displayed by V_{eff} as following,

$$V_{eff} = V_{ext}(\vec{r}) + V_{ee}(\vec{r}) + V_{xc}(\vec{r}) \quad (2.4.7)$$

Then the Kohn-Sham equation could be rewritten as following,

$$\left[-\frac{1}{2}\nabla^2 + V_{eff}(\vec{r}) \right] \psi_i(\vec{r}) = \varepsilon_i \psi_i(\vec{r}) \quad (2.4.8)$$

Both of V_{eff} and T_s in equation (2.4.8) are the functional of density. By given $\rho_{in}(\vec{r})$, Hamiltonian operator could be obtained. Beside, both ε_i and ψ_i could be calculated by equation (2.4.8). Applying ψ_i in to equation (2.4.3), $\rho_{out}(\vec{r})$ could be acquired. The initial density, $\rho_{in}(\vec{r})$, could be given until $\rho_{in}(\vec{r}) = \rho_{out}(\vec{r})$. When $\rho_{in}(\vec{r}) = \rho_{out}(\vec{r})$, equation (2.4.8) was solved, and ε_i is the energy of ground state.

2.5 Optimization of geometry and vibrational frequency

The energy of a molecule is dependent on the position of the nuclei in the system. In other words, the energy of the system is dependent on geometry of the molecule. For a non-linear molecule composed of N atoms, it has $3N-6$ vibrational degrees of freedom, and for a linear molecule, it has $3N-5$ degrees of freedom, thus the energy of the system could be thought as a curved many-dimensional surface. The main goal of optimization is to find the minimum on the surface.

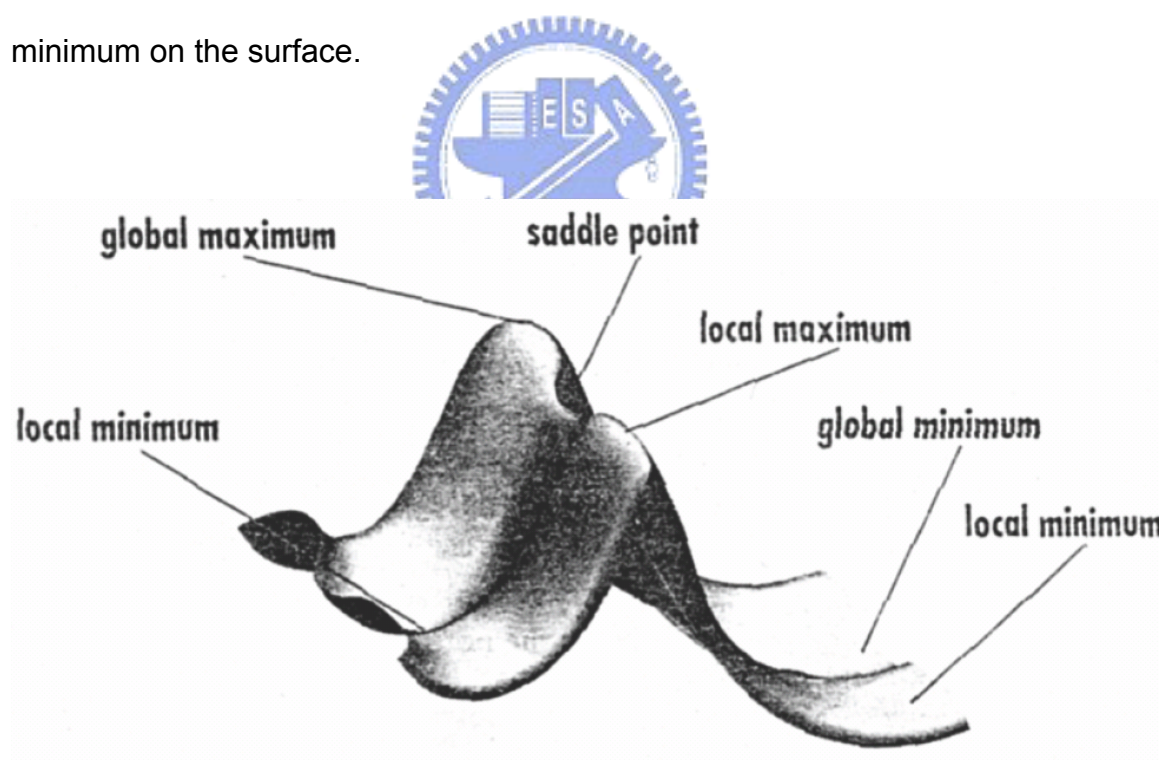
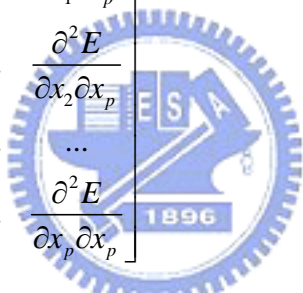


Figure 2.5.1 Potential energy surface (PES) of a molecule[12].

In figure 2.5.1, there is a minimum point in the whole region and it is called

global minimum. At the global minimum point, the most stable geometry could be found having the lowest energy. There are two conditions which have to be satisfied at this point. First one, $\frac{\delta E}{\delta r}$ must equal to zero, but it is also satisfied with any minimum or maximum even at a saddle point; thus to find the global minimum point, another condition is needed, $\frac{\delta^2 E}{\delta r^2}$ must larger be than or equal to zero. There are various r value in a many-body system, thus $\frac{\delta^2 E}{\delta r^2}$ is rewritten as a matrix which is also called Hessian matrix.

$$H = \begin{bmatrix} \frac{\partial^2 E}{\partial x_1 \partial x_1} & \frac{\partial^2 E}{\partial x_1 \partial x_2} & \dots & \frac{\partial^2 E}{\partial x_1 \partial x_p} \\ \frac{\partial^2 E}{\partial x_2 \partial x_1} & \frac{\partial^2 E}{\partial x_2 \partial x_2} & \dots & \frac{\partial^2 E}{\partial x_2 \partial x_p} \\ \dots & \dots & \dots & \dots \\ \frac{\partial^2 E}{\partial x_p \partial x_1} & \frac{\partial^2 E}{\partial x_p \partial x_2} & \dots & \frac{\partial^2 E}{\partial x_p \partial x_p} \end{bmatrix} \quad (2.5.1)$$


Vibrational motions can be calculated by computing the result of Hessian matrix, and an infrared spectrum could be predicted by the Hessian matrix, furthermore make sure the optimization result.

A transition state geometry could be found by the same method, and the only difference is that the predicted result of the Hessian matrix has a negative frequency on the chosen freedom. Only the transition state has an imaginary frequency with a stable structure. Transition states (TS) locate on the maxima of a PES, thus energy is decreased with the molecule changing along its

vibrational direction of the imaginary frequency.

The intrinsic reaction coordinate (IRC)[13] method is typically used to find and to insure that reactants are connected products via the TS. The energy is calculated along the vibrational direction of the imaginary frequency, and the reactants and products could be determined by optimizing geometries on both sides of the maximum point.



3. Results and discussion

3.1 Reactions of Trimethylaluminum (CH₃)₃Al and Oxygen

In this reaction (CH₃)₂AlO₂ is a potential product and the CH₃ radical is a potential reactive product which may initiate a chain reaction in air. The detail of the explosive reaction initiated by CH₃ was mentioned in Chapter 1.

All the steps involved in this reaction were searched by using various methods, B3LYP, MP2, CCSD, CCSD(T) and G2M. All the optimized geometries were derived by B3LYP/6-311++G(3df,2p) shown in Figure 3.1.1. The structures of the reactants, intermediates, transition states and products obtained by both B3LYP/6-311++G(3df,2p) and MP2/6-311++G(d,p) methods shown in Table 3.1.1. The C^a atom in Table 3.3.1 represents the carbon which was broken from TMAI to form CH₃. All relative energies of the gas-phase species derived by different methods are listed in Table 3.1.2. The potential energy diagram of this reaction as shown in Figure 3.1.2 was obtained from the calculation at CCSD(T)/6-311+G(3df,2p)//B3LYP/6-311++G(3df,2p) level of theory. All of the energies were evaluated relative to the reference state: TMAI + O₂.

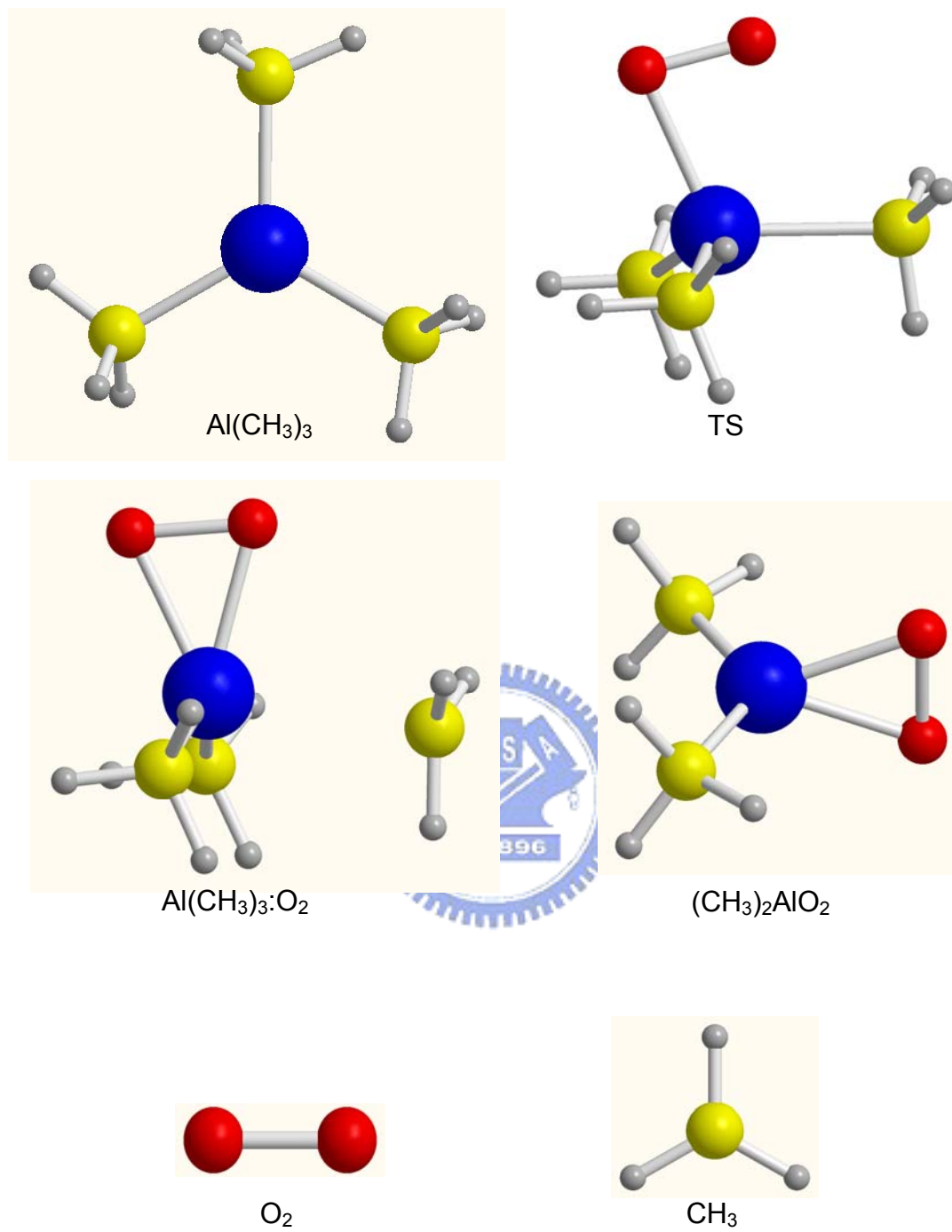


Figure 3.1.1 Optimized geometries of species involved in reaction TMAI + O₂

B3LYP/6-311++g(3df,2p)
MP2/6-311++g(d,p)
CCSD/6-31+g(d,p)
CCSD(T)/6-311+g(3df,2p)//B3LYP/6-311++g(3df,2p)
G2M

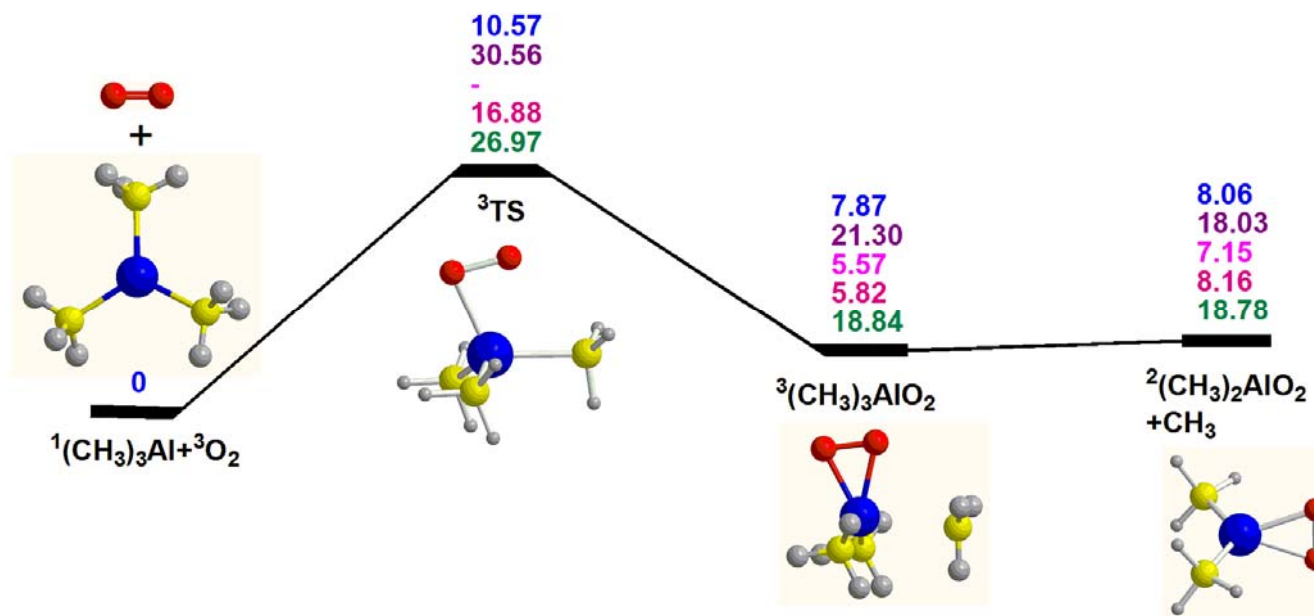


Figure 3.1.2 Potential energy surface of the TMAI + O_2 reaction

Table 3.1.1 Geometrical details of all species in reaction TMAI + O₂ (Å)

Species	(CH ₃) ₃ Al+O ₂	TS	³ (CH ₃) ₃ AlO ₂	² (CH ₃) ₂ AlO ₂ +CH ₃
R(Al-C) B3LYP	1.97	1.97	1.96	1.95
R(Al-C ^a) B3LYP	1.97	2.12	2.61	-
R(Al-O) B3LYP	-	2.00	1.93	1.89
R(O-O) B3LYP	1.20	1.29	1.34	1.35
R(Al-C) MP2	1.97	1.96	1.95	1.95
R(Al-C ^a) MP2	1.97	2.11	2.91	-
R(Al-O) MP2	-	2.02	1.90	1.90
R(O-O) MP2	1.22	1.30	1.38	1.37

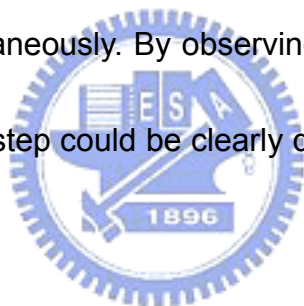
Table 3.1.2 Species relative energy in reaction TMAI + O₂ (kcal/mol)

Species	(CH ₃) ₃ Al+O ₂	TS	³ (CH ₃) ₃ AlO ₂	² (CH ₃) ₂ AlO ₂ +CH ₃
B3LYP/6-311++g(3df,2p)	0.0	10.57	7.87	8.06
MP2/6-311++g(d,p)	0.0	30.56	21.30	18.03
CCSD/6-31+g(d,p)	0.0	-	5.57	7.15
CCSD(T)/6-311+g(3df,2p) //B3LYP/6-311++g(3df,2p)	0.0	16.88	5.82	8.16
G2M	0.0	26.97	18.84	18.78

As shown in Figure 3.1.2, a stable intermediate could not be directly produced from the TMAI reactive with O₂. It is different from the reaction between TMAI and water will be discussed in the section 3.3.2. In the reaction of TMAI and H₂O, a stable intermediate is formed by binding TMAI and H₂O.

To form (CH₃)₃AlO₂ from TMAI + O₂, a transition state must be overcome

(shown in Figure 3.1.2). After that, O_2 is bound with the aluminum atom at the center of TMAI molecule to form $(CH_3)_3AlO_2$. The predicted geometries provide a useful information on the reaction mechanism. From Table 3.1.1, the bond length of Al-C was about 1.97 Å in the TMAI molecule. The distance almost remains the same with transition state. The distance between Al and C^a lengthens from 1.97 to 2.12 Å, as the reaction proceeds. One of the oxygen double bonds is broken in this step because the distance between two oxygen atoms is increased from 1.20 to 1.29 Å, and the aluminum is bound with oxygen simultaneously. By observing the bond length change, in Al- C^a , O-O and Al-O, this step could be clearly defined as the critical motions of the transition state.



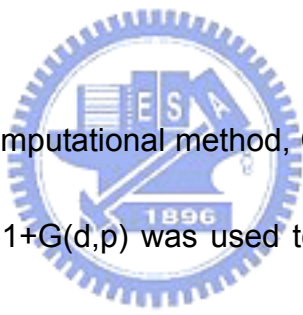
To form the final products, $(CH_3)_2AlO_2$ and CH_3 , one of the CH_3 groups must be ejected from $(CH_3)_3AlO_2$ as shown in Figure 3.3.2. The carbon atom which is later expelled from Al called C^a . The Al- C^a bond length was about 2.61 Å in $(CH_3)_3AlO_2$ (shown in Table 3.3.1), it indicates that this Al- C^a bond is much weaker than the other two Al-C bonds. As the PES has shown, by giving energy at most 3 kcal/mol, this Al- C^a bond could be broken to form the free methyl radical. With the final products formed, the Al-C bond length is shortened to 1.95 Å in $(CH_3)_2AlO_2$, and the distance of Al-O is also decreased

to 1.89 Å. In this regard, the binding energy of Al-O is stronger in $(\text{CH}_3)_2\text{AlO}_2$ than in $(\text{CH}_3)_3\text{AlO}_2$ as one would expect. The O-O bond length is increased to 1.35 Å in the $(\text{CH}_3)_2\text{AlO}_2$ product.

B3LYP and MP2 were chosen to carry out the calculation for the whole PES of the reaction between TMAI and O_2 . The predicted energies by MP2 were always higher than those by B3LYP. The energy differences between MP2 and B3LYP were about 20, 14, and 10 kcal/mol in each step (shown in Table 3.1.2). It is worth noting that for the transition state, the difference in relative energies between MP2 and B3LYP was as high as 19.99 kcal/mol. The geometries and imaginary frequencies were later checked to clarify why the energies of transition state calculated by the two methods were so different. The geometries of the transition state obtained by MP2 and B3LYP were only slightly different (compared in Table 3.1.1), but the imaginary frequencies were found to be significantly different, that computed by MP2 was 1197.26 cm^{-1} , which is higher than that predicted by B3LYP by 201.43 cm^{-1} . It should be noted that both transition states were examined by IRC; not only the result of the forward IRC went to the identical products but also the result of the reverse IRC went to the same reactants. To improve the energy prediction, higher level methods were used to re-calculate this reaction as

discussed below.

Two higher levels of theory including the G2M method were utilized to improve the energetics. It turns out that most of the energies lie between MP2 and B3LYP as shown in Table 3.1.2. The G2M method is a composite scheme, which involves with B3LYP, MP4, MP2, and CCSD(T) methods based on the MP4 value. In other words, the result obtained from G2M was still influenced significantly by MP4. It may be the reason that the PES predicted by G2M was still higher than that by B3LYP but slightly lower than that by MP2.



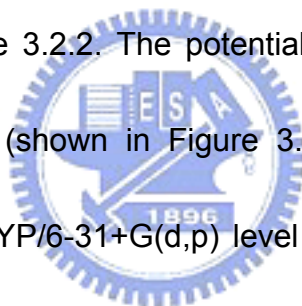
Another higher-level computational method, CCSD, was used to compute the PES again. CCSD/6-31+G(d,p) was used to optimize each state again. The obtained relative energies were close to that from B3LYP except for the transition state (not calculated yet). In summary, the results obtained by CCSD and B3LYP methods were almost identical. The higher level method, CCSD(T) single point calculation, was later chosen to re-calculate the geometries which were acquired by B3LYP/6-311++G(3df,2p). All of the three computational methods, B3LYP/6-311++G(3df,2p), CCSD/6-31+G(d,p), and CCSD(T)/6-311G+(3df,2p)//B3LYP/6-311++G(3df,2p) had almost the same result as shown in Table 3.1.2.

From the aforementioned results, the reaction between TMAI and O₂ has a relatively low energy barrier, about 17 kcal/mol, as shown in Table 3.1.2. The final products are (CH₃)₂AlO₂ and CH₃ radical; if formed they can lead to a sustained reaction in the air.



3.2 Reactions of Trimethylaluminum (CH₃)₃Al and water

We used two different methods, scilicet B3LYP and MP2, to carry out the calculation for all the reaction steps. All the optimized geometries were predicted by B3LYP/6-31+G(d,p) as shown in Figure 3.2.1, and the structures of the reactants, intermediates, transition states and produces by both B3LYP/6-31+G(d,p) and MP2/6-31+G(d,p) methods as presented in Table 3.2.1. The H^a atom in Table 3.2.1, represents the Hydrogen atom binding with Oxygen. All relative energies of the gas-phase species obtained by different methods are listed in Table 3.2.2. The potential energy diagram of reaction between TMAI and water (shown in Figure 3.2.2) was obtained from the CCSD(T)/6-31+G(d,p)//B3LYP/6-31+G(d,p) level calculation. All the energies were calculated with reference to the reactants: TMAI + H₂O.



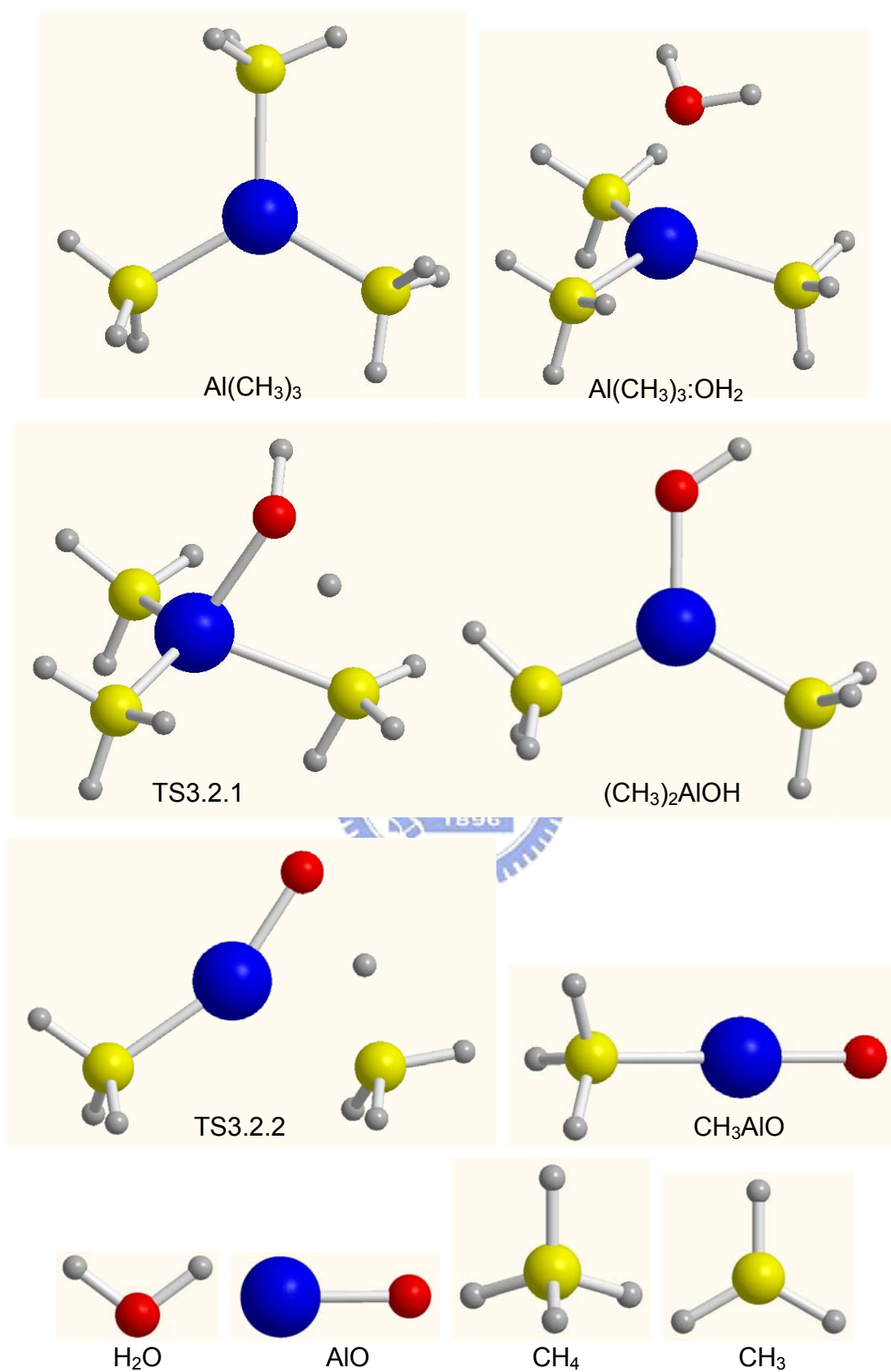


Figure 3.2.1 Optimized geometries of species involved in reaction TMAI + H₂O

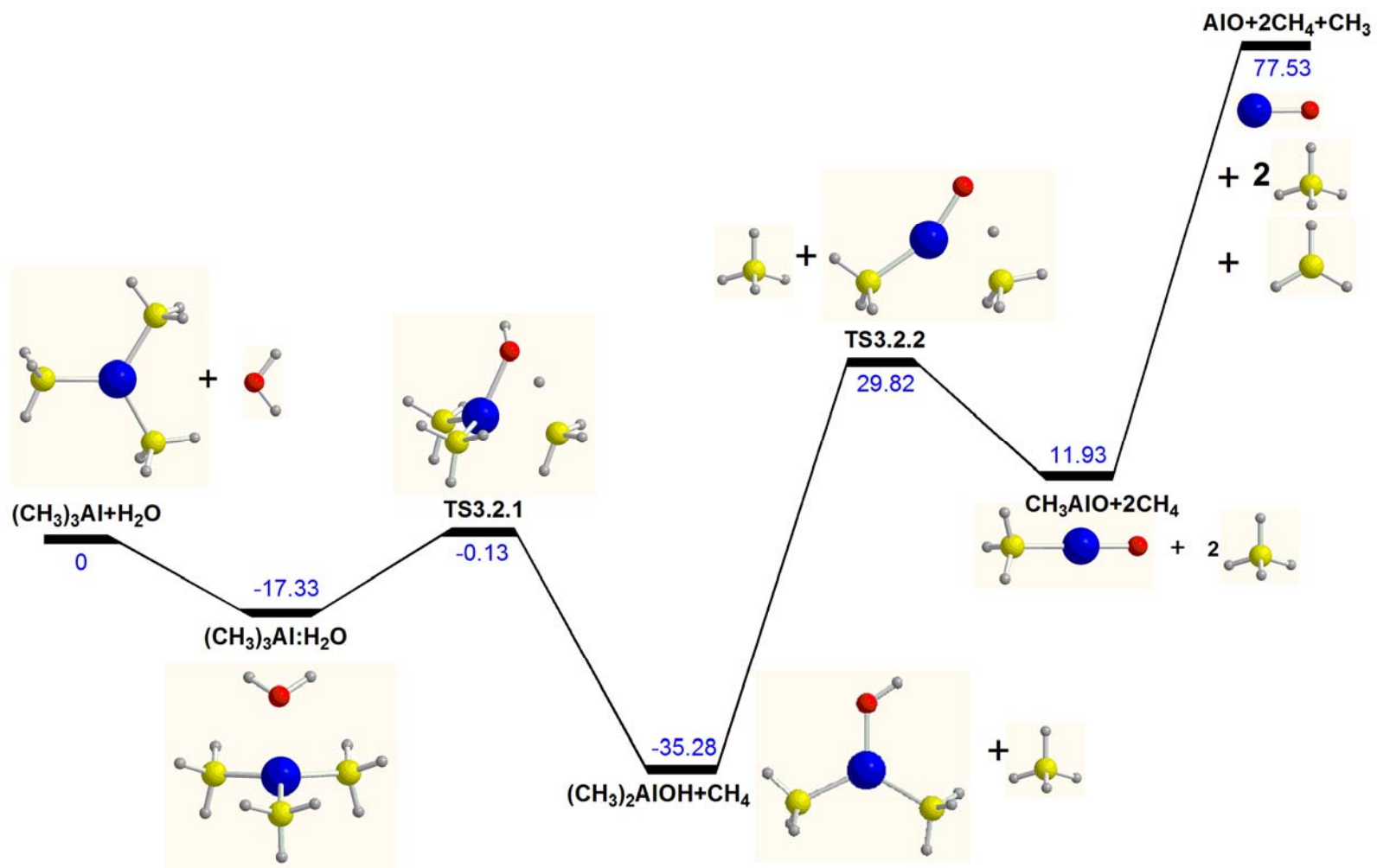


Figure 3.2.2 Potential energy surface of reaction TMAI + H₂O

Table 3.2.1 Geometrical details of all species in reaction TMAI + H₂O (Å)

Species	(CH ₃) ₃ Al	(CH ₃) ₃ Al:H ₂ O	TS3.2.1	(CH ₃) ₂ AlOH	TS3.2.2	CH ₃ AlO	AlO
R(Al-C) B3LYP	1.97	1.98	2.17	1.96	2.23	1.95	-
R(Al-O) B3LYP	-	2.12	1.93	1.73	1.66	1.62	1.65
R(O-H) B3LYP	-	0.97	1.18	0.96	1.45	-	-
R(C-H ^a) B3LYP	-	2.95	1.96	3.37	1.33	-	-
A(C-Al-C) B3LYP	120.2	118.2	110.6	125.2	115.3	-	-
A(C-Al-O) B3LYP	-	96.7	79.3	119.4	87.0	180.0	-
R(Al-C) MP2	1.97	1.98	2.15	1.96	2.20	1.95	-
R(Al-O) MP2	-	2.101	1.93	1.74	1.68	1.64	1.62
R(O-H) MP2	-	0.97	1.18	0.96	1.44	-	-
R(C-H ^a) MP2	-	2.92	1.48	3.37	1.32	-	-
A(C-Al-C) MP2	120.1	118.1	109.9	125.1	114.6	-	-
A(C-Al-O) MP2	-	96.1	79.0	119.8	87.1	180.0	-

Table 3.2.2 Species relative energy in reaction TMAI + H₂O (kcal/mol)

Species	Reactants	(CH ₃) ₃ Al:H ₂ O	TS3.2.1	(CH ₃) ₂ AlOH +CH ₄	TS3.2.2 +CH ₄	CH ₃ AlO +2CH ₄	AlO+2CH ₄ +CH ₃
B3LYP/6-31+G(d,p)	0	-11.30	1.63	-35.09	26.68	9.92	74.76
MP2/6-31+G(d,p)	0	-15.13	0.19	-36.03	25.61	6.15	90.34
CCSD(T)/6-31+G(d,p) //B3LYP/6-31+G(d,p)	0	-17.33	-0.13	-35.28	29.82	11.93	77.53
CCSD(T)/6-31+G(d,p) //MP2/6-31+G(d,p)	0	-15.00	2.20	-34.97	30.01	9.98	75.58

Trimethylaluminum has a planar structure with rotational energy barriers for the methyl groups. This implies that one Al 3s and two Al 3p orbitals hybridize to form three sp^2 orbitals bonding with $-CH_3$ ligands, and an empty p orbital was left on the Al atom[14]. The bond length between C and Al is

predicted to be 1.98 Å.

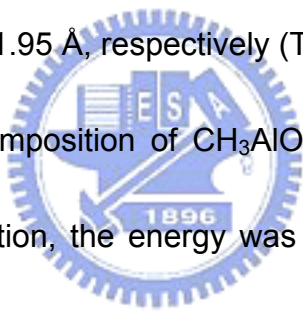
For the reaction between $\text{Al}(\text{CH}_3)_3$ and H_2O , the empty p orbital of TMAI can interact with the incoming H_2O lone pair electron[14] to form a molecular complex, i.e., $(\text{CH}_3)_3\text{Al}:\text{OH}_2$ as shown in Figure 3.2.1. Complexation with a water molecule yields a stable complex structure, $(\text{CH}_3)_3\text{Al}:\text{OH}_2$, with 11.3 kcal/mol or 15.1 kcal/mol binding energy calculated on the B3LYP/6-31+G(d,p) or the MP2/6-31+G(d,p) method, respectively. The binding energy has also been computed by CCSD(T)//B3LYP and CCSD(T)//MP2; -17.3 kcal/mol and -15.0 kcal/mol, respectively. As shown in Figure 3.2.1, the water molecule was formed to locate above the trimethylaluminum plane through the interaction between the lone pair electron of H_2O and empty p orbital of the Al atom in trimethylaluminum. The bond length between the Al atom and the oxygen atom is 2.12 Å. This value is close to the distance between Al and O atoms when TMAI is bonding with an $-\text{OH}$ ligand on the silicon surface[15]. In the present case the $(\text{CH}_3)_3\text{Al}:\text{OH}_2$ complex has C_1 symmetry, and the angle C-Al-C changes by more than 1° from 120.2° in TMAI to 118.2° in $\text{TMAI}:\text{OH}_2$. According to the potential energy surface (Figure 3.2.2) $(\text{CH}_3)_3\text{Al}:\text{OH}_2$ the intermediate is seen to be easy to form.

The decomposition of the $(\text{CH}_3)_3\text{Al}:\text{OH}_2$ intermediate may produce CH_4

and the stable molecule, $(\text{CH}_3)_2\text{AlOH}$. In the reaction, one of the two H atoms of water interacts with one of the CH_3 ligands at TS3.2.1, in which the angle O-Al-C decreases to a value less than 90° and the bond length between O and Al atoms decreases from 2.12 Å to 1.93 Å. The transition vector is dominated by the migration of hydrogen which is 1.18 Å away from O atom and 1.96 Å away from the interacting C atom; the Al-C bond is elongated from 1.98 Å to 2.17 Å. The barrier at TS3.2.1 was predicted to 17.17 kcal/mol above the complex (or 0.13 kcal/mol below the reactants) the CCSD(T)/6-31+G(d,p)//B3LYP/6-31+G(d,p) calculation. The formation of $(\text{CH}_3)_2\text{AlOH}$ and CH_4 from TS3.2.1 was found to be exothermic by 35.17 kcal/mol and 37.2 kcal/mol basic on CCSD(T)//B3LYP and CCSD(T)//MP2, respectively.

The $(\text{CH}_3)_2\text{AlOH}$ molecule can further to give another CH_4 and CH_3AlO (as shown in Figure 3.2.1) with a very large energy barrier (29.82 kcal/mol) at TS3.2.2. The O-Al-C angle at TS3.2.2 was formed to decrease from 116.4 in $(\text{CH}_3)_2\text{AlOH}$ to 87.0 in TS3.2.2. This also suggests that the transition vector is dependent on the motion of hydrogen. This action was similar with TS3.2.1. From the TS3.2.2 geometry (see Table 3.2.1), it is easy to notice that the distance from H atom to oxygen is 1.45 Å and from H atom to carbon is 1.33Å.

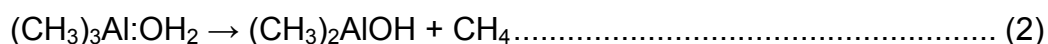
The Al-C bond length is extended from 1.96 Å to 2.23 Å, which is a significant change. The evolution from TS3.2.2 to CH₃AlO leads to the ejection of the CH₄ molecule release of 18.9 kcal/mol and 20.0 kcal/mol energy according to the CCSD(T)//B3LYP and CCSD(T)//MP2 methods, respectively. The overall endothermicity of the reaction product CH₃AlO + 2CH₄ was predicted to be 11.9 kcal/mol and 10 kcal/mol above the reactants by using CCSD(T)//B3LYP and CCSD(T)//MP2, respectively. CH₃AlO has a C_{3v} symmetry with the angle of C-Al-O changing from 120° to 180°. The bond lengths of Al-O and Al-C were computed to be 1.62 Å and 1.95 Å, respectively (Table 3.2.1).



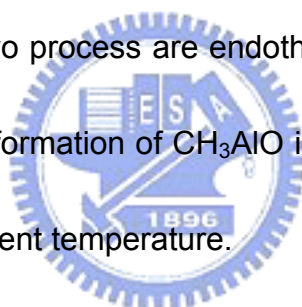
Furthermore, the decomposition of CH₃AlO given two doublet radicals, CH₃ and Al-O. In this reaction, the energy was formed to be 65.6 kcal/mol, according to CCSD(T)//B3LYP and CCSD(T)//MP2 calculation. The doublet electronic ground state of AlO has a bond length of 1.65 Å, which was longer than that in CH₃AlO (1.62 Å). In the potential energy surface shown in Figure 3.2.2, the predicted energy for the final products is around 77.5 kcal/mol and 75.6 kcal/mol above the reactants based on CCSD(T)//B3LYP and CCSD(T)//MP2, respectively.

The association reaction of trimethylaluminum with H₂O can give rise to molecular complexes, (CH₃)₃Al:OH₂. Overall, both DFT and ab initio methods

with the correlation energy correction seem to have a good agreement in geometries and relative energies. The overall reaction mechanisms for these reactions can be written as follows:



In these reaction, the first two reactions are exothermic and can occur readily, whereas the last two process are endothermic and thus cannot occur readily. The barrier for the formation of CH_3AlO is 29.8 kcal/mol which cannot be easily overcome at ambient temperature.



3.3 Reactions of Dimethylaluminum (CH₃)₂Al and water

All the geometries of the reactants, intermediates, transition states and products were optimized using B3LYP/6-31+G(d,p) and MP2/6-31+G(d,p), and the structures are shown in Figure 3.3.1 using those from B3LYP/6-31+G(d,p). The detailed data of these geometries were listed in the Table 3.3.1. In this Table the H^a atom represents the H atom binding with Oxygen in the water molecule. Potential energy surface of the H₂O + DMAI reaction is shown in Figure 3.3.2, and relative energies (kcal/mol) calculated by CCSD(T)/6-31+G(d,p)//B3LYP/6-31+G(d,p) + ZPVE level of theory are listed in Table 3.3.2.



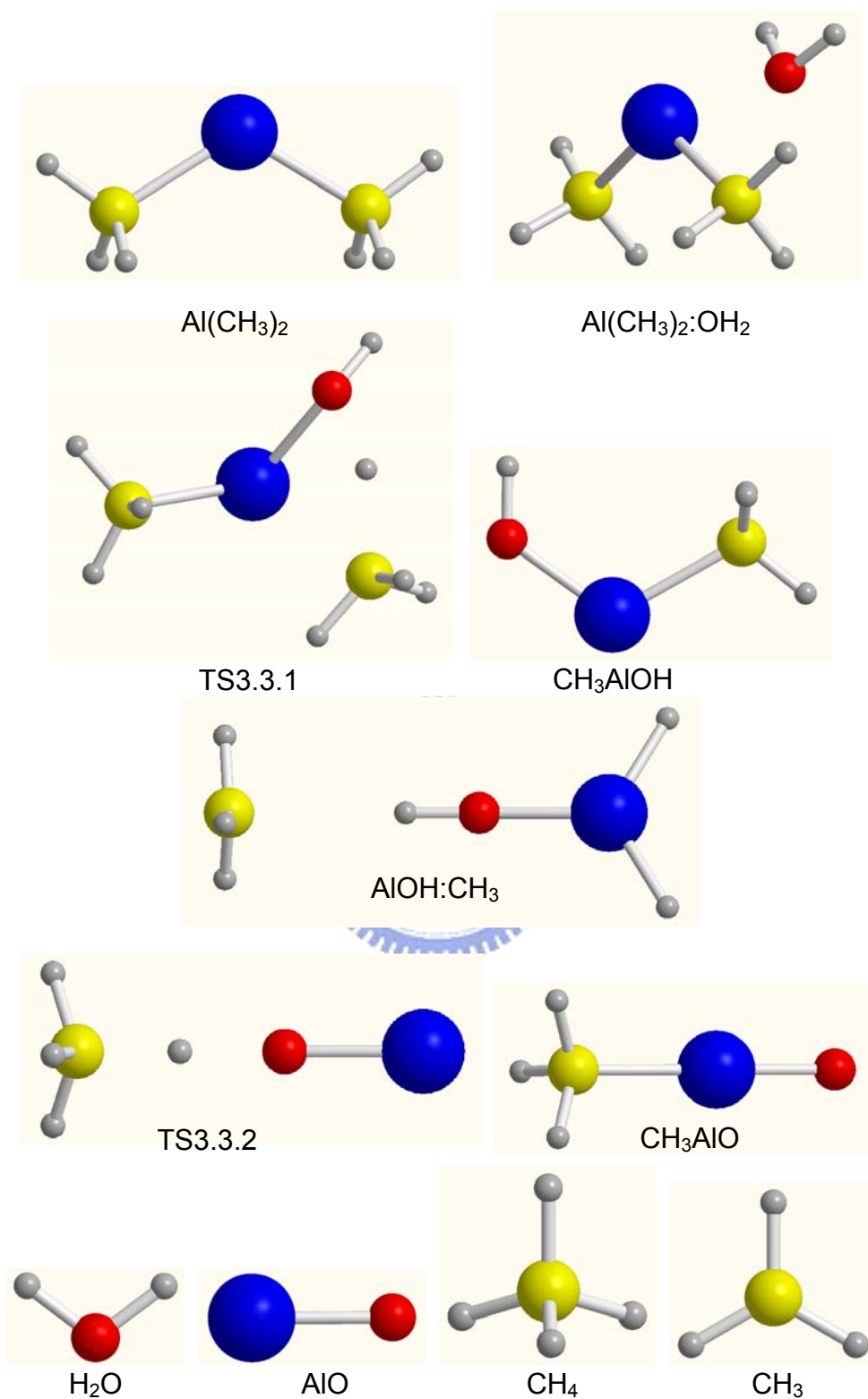


Figure 3.3.1 Optimized geometries of species involved in reaction $\text{DMAI} + \text{H}_2\text{O}$

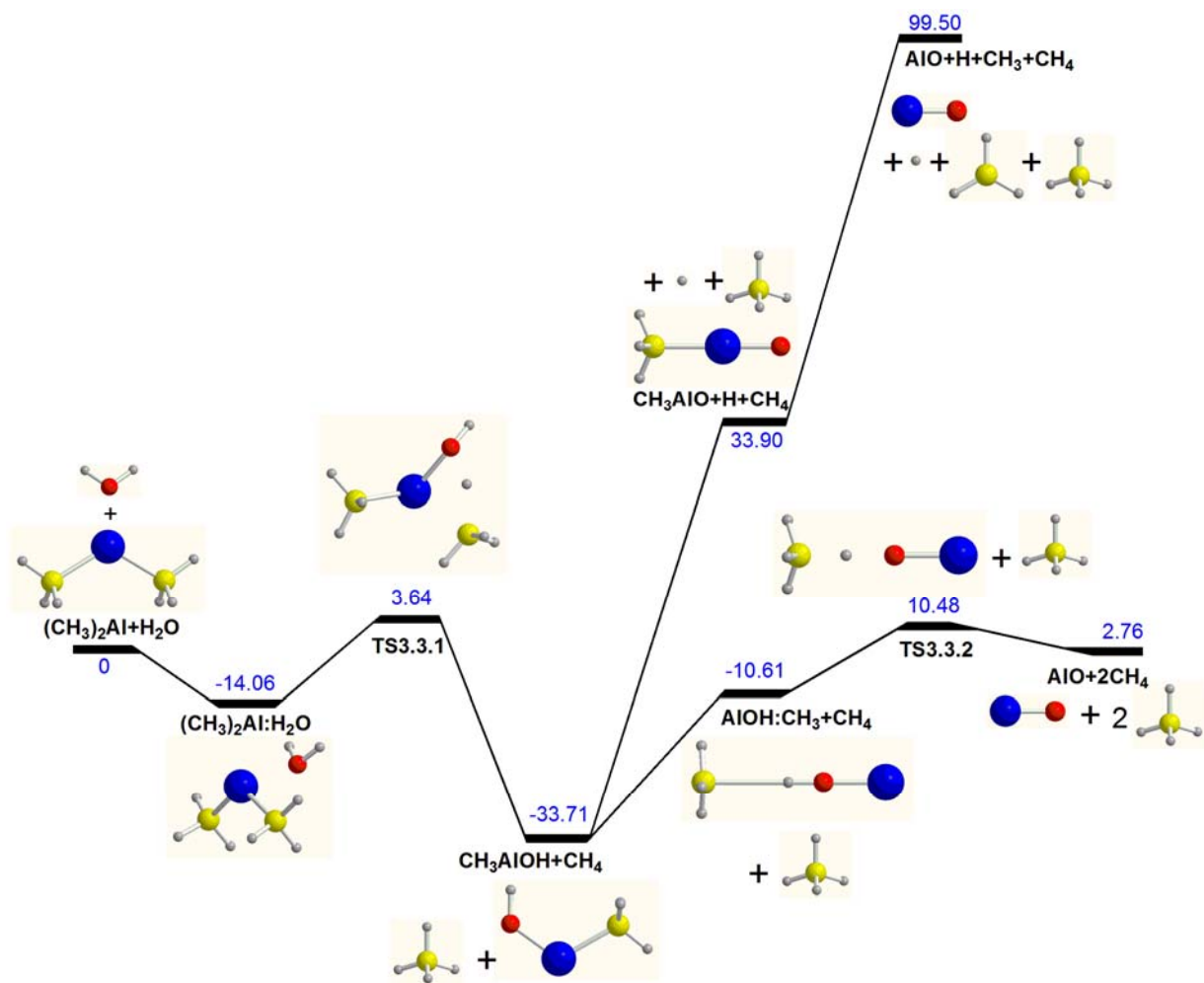


Figure 3.3.2 Potential energy surface of reaction DMAI + H₂O

Table 3.3.1 Geometrical details of all species in reaction DMAI + H₂O (Å)

Species	Reactants (CH ₃) ₂ Al:H ₂ O		TS3.3.1	CH ₃ AlOH +CH ₄	AlOH:CH ₃ +CH ₄	TS3.3.2	AlO+2CH ₄	CH ₃ AlO +CH ₄ +CH ₃ +H
R(Al-C) B3LYP	1.99	1.99	2.19	1.99	-	-	-	1.95
R(Al-O) B3LYP	-	2.13	1.94	1.73	1.70	1.69	1.65	1.62
R(O-H) B3LYP	0.97	0.97	1.19	0.96	0.96	1.28	-	-
R(C-H ^a) B3LYP	-	3.25	1.48	2.42	2.32	1.26	-	-
A(C-Al-C) B3LYP	120.2	119.1	111.5	-	-	-	-	-
A(C-Al-O) B3LYP	-	96.6	78.2	114.8	-	-	-	180.0
R(Al-C) MP2	1.98	1.99	2.17	1.98	-	-	-	1.95
R(Al-O) MP2	-	2.12	1.94	1.74	1.71	1.69	1.62	1.64
R(O-H) MP2	0.97	0.97	1.19	0.96	0.96	1.40	-	-
R(C-H ^a) MP2	-	3.22	1.47	2.43	2.41	1.17	-	-
A(C-Al-C) MP2	120.1	119.4	110.7	-	-	-	-	-
A(C-Al-O) MP2	-	96.3	78.3	119.7	-	-	-	180.0

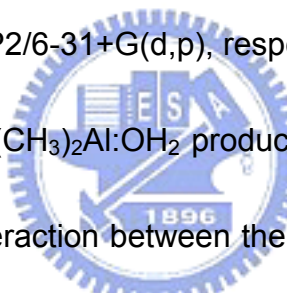
 Table 3.3.2 Species relative energy in reaction DMAI + H₂O (kcal/mol)

Species	Reactants (CH ₃) ₂ Al:H ₂ O		TS3.3.1	CH ₃ AlOH +CH ₄	AlOH:CH ₃ +CH ₄	TS3.3.2	AlO+2CH ₄	CH ₃ AlO +CH ₄ +CH ₃ +H
B3LYP/6-31+G(d,p)	1.99	1.99	2.19	1.99	-	-	-	1.95
MP2/6-31+G(d,p)	-	2.13	1.94	1.73	1.70	1.69	1.65	1.62
CCSD(T)/6-31+G(d,p) //B3LYP/6-31+G(d,p)	0.97	0.97	1.19	0.96	0.96	1.28	-	-
CCSD(T)/6-31+G(d,p) //MP2/6-31+G(d,p)	-	3.25	1.48	2.42	2.32	1.26	-	-

The decomposition of TMAI to DMAI may occur under certain conditions, for example, in a CVD experiment which may be carried out in a heated reactor. The result of TMAI decomposition forms DMAI and CH₃. The heat of decomposition was estimated to be 74.8 kcal/mol using both

B3LYP/6-31+G(d,p) and CCSD(T)//B3LYP methods. Dimethylaluminum is expected to react readily as discussed below.

As shown in Figure 3.3.2, DMAI reacts with H₂O to form first the molecular complex, (CH₃)₂Al:OH₂. This reaction is a barrierless process. In the initial step, the O atom in H₂O directly associated with the Al atom in (CH₃)₂Al to form the complex; and the process is exothermic by 14.1 kcal/mol at the CCSD(T)/6-31+G(d,p)//B3LYP/6-31+G(d,p) level of theory. The bond length between the O and Al atoms are 2.13 and 2.12 Å based on the B3LYP/6-31+G(d,p)]and MP2/6-31+G(d,p), respectively.



The decomposition of (CH₃)₂Al:OH₂ produces CH₄ and the stable radical product, CH₃AlOH. The interaction between the H atom of H₂O and the -CH₃ ligand at TS3.3.1 decreases the bond length of O-Al from 2.13 Å to 1.94 Å by the B3LYP/6-31+G(d,p) method. The angle of C-Al-C changes from 119.1° to 111.5°. This implies that the critical factor to form TS3.3.2 is dependent on the migration of the H atom of H₂O. The barrier at TS3.3.2 was predicted to be 17.7 kcal/mol (or 3.6 kcal/mol above the reactants) based on the CCSD(T)//B3LYP level of calculation. In the distance between the C and Al atoms is expanded along their bond length vector, and one CH₄ is eliminated from DMAI:OH₂ via TS3.3.2 to give CH₃AlOH. In this step, around 30 kcal/mol

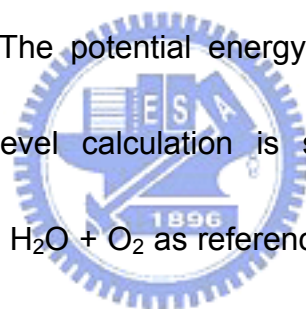
energy will be released on the basis of the CCSD(T)//B3LYP level calculation.

The Al-O bond length was decreases again from 1.94 Å to 1.73 Å.

CH₃AlOH may decompose to another intermediate CH₃AlO and H, and the Al-O bond length of CH₃AlO, 1.62 Å is little shorter than that in AlCH₃OH (about 0.02 Å by the B3LYP/6-31+G(d,p) method). The dissociative process requires 67.6 kcal/mol of energy. From the geometry of CH₃AlO, it can be clearly seen that the molecule is linear, CH₃AlO may decompose to two doublet radicals, AlO and CH₃. In addition, CH₃AlOH was formed to isomerize to AlOH:CH₃ with 23.1 kcal/mol endothermicity (see Figure 3.3.2). A similar complex has been reported before for InOHCH₃ by Tseng et al[16]. The AlOHCH₃ complex can readily decompose via TS3.3.2 by increasing the bond length of O-H; at TS3.3.2 O-H distance is extended by 0.31 Å from 0.963 Å to 1.28 Å when intermediate AlOHCH₃ decompose via TS3.3.2 based on the B3LYP/6-31+G(d,p). In this step, the activation energy is estimated to be 21.1 kcal/mol. The overall endothermicity for the formation of Al + 2CH₄ is predicted to be 2.5kcal/mol.

3.4 Reaction of Trimethylaluminum, O₂ and H₂O

The geometries of the reactants, intermediates, transition states and products in this reaction were optimized by B3LYP/6-311++G(3df,2p), and the structures are shown in Figure 3.4.1. More detailed computational results of these geometries are summarized in Table 3.4.1. In the table the atom C^a represents the methyl which is to be separated from the Aluminum and the O^a atom represents the oxygen atom in the oxygen molecule attached to the Al atom. All relative energies of gas-phase species derived by different methods are listed in Table 3.4.2. The potential energy diagram obtained from the B3LYP/6-311++G(3df,2p) level calculation is shown in Figure 3.4.2. By regarding reactants TMAI + H₂O + O₂ as reference state, all the relative levels of energy are calculated relative comparison to the reference state.



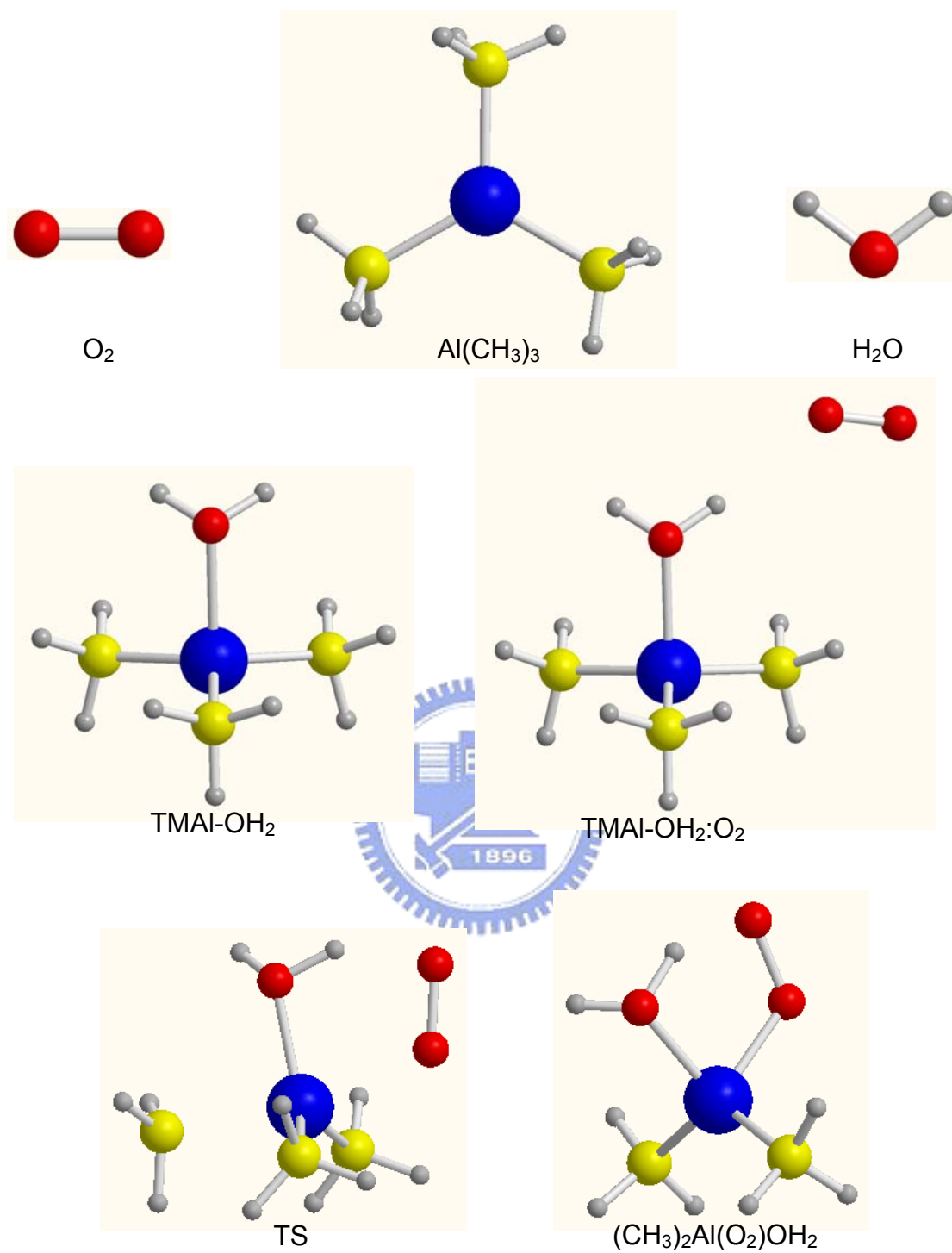


Figure 3.4.1 The optimized geometries of reaction $TMAI + O_2 + H_2O$

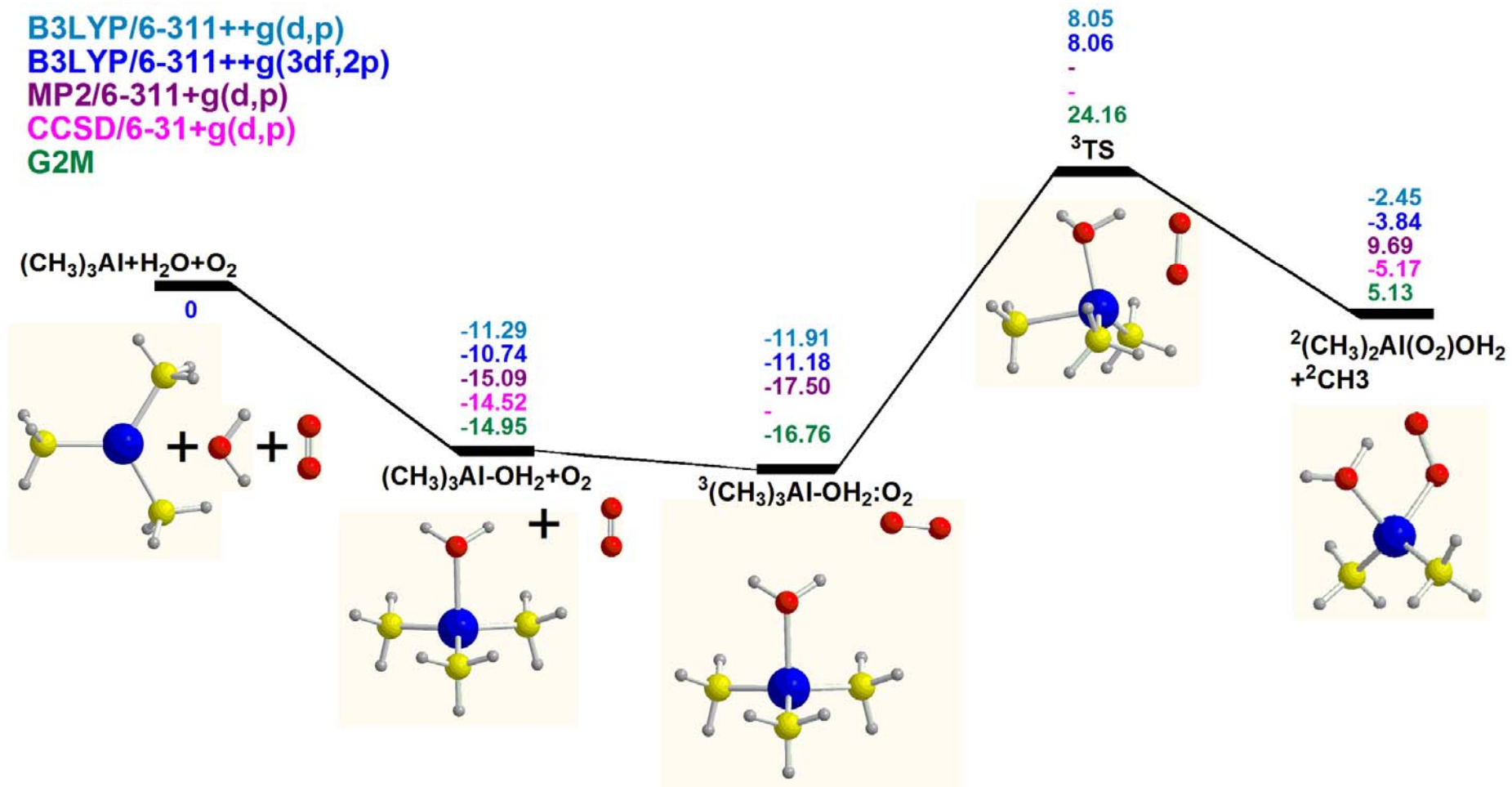


Figure 3.4.2 Potential energy surface of reaction TMAI + O₂ + H

Table 3.4.1 Geometrical details of species in reaction TMAI + O₂ + H₂O

Species	Reactants	TMAI-OH ₂	TMAI-OH ₂ :O ₂	TS	(CH ₃) ₂ Al(O ₂)OH ₂ +CH ₃
R(Al-C)	1.97	1.97	1.98	1.99	1.95
R(Al-C ^a)	1.97	1.98	1.99	2.16	-
R(Al-O)	-	2.09	2.08	1.94	1.92
R(Al-O ^a)	-	-	5.13	2.22	1.91
R(O-H)	0.96	0.96	0.97	1.54	1.06
R(O ^a -O ^a)	1.20	1.20	1.20	1.28	1.32
A(C-Al-C)	119.95	117.90	117.53	131.09	124.91
A(C-Al-O)	-	96.13	97.87	112.16	110.04

Table 3.4.2 Species relative energy in reaction TMAI + O₂ + H₂O (kcal/mol)

Species	Reactants	TMAI-OH ₂	TMAI-OH ₂ :O ₂	TS	(CH ₃) ₂ Al(O ₂)OH ₂ +CH ₃
B3LYP/++6-311G(d,p)	0	-11.29	-11.91	8.05	-2.45
B3LYP/++6-311G(3df,2p)	0	-10.74	-11.18	8.06	-3.84
MP2/+6-311G(d,p)	0	-15.09	-17.50	-	9.69
CCSD/+6-31G(d,p)	0	-14.52	-	-	-5.17
G2M	0	-14.95	-16.76	24.16	5.13

At first, B3LYP/6-311++G(d,p) was employed to map the whole PES. Then the higher level basis set 6-311++G(3df,2p) was applied to improve the energies. The PESs obtained by both basis sets are almost the same. Other levels of computational methods should be applied to confirm the energy levels again. In this regard, MP2/6-311+G(d,p) was chosen to calculate the same reaction. The relative energies of final products by MP2 are higher than that obtained by B3LYP. To double-check the reliability of results, G2M was used to

compute out the whole PES again. The G2M method is a mixed method, and it involves B3LYP, MP4, MP2, and CCSD(T) methods so the relative energies from G2M are lie between MP2 and B3LYP. It means that G2M is still affected by MP2 significantly. The whole PES of this reaction may be optimized again by the CCSD method. The result obtained from CCSD appears to be similar with that obtained from B3LYP. The following discussion will be focused on the results from B3LYP and CCSD.

In this reaction, the water molecule is used as a catalyst to slightly help O₂ molecule bind with TMAI. The TMAI will be bound with H₂O at first with about 14 kcal/mol exothermicity; the geometries of both the TMAI and H₂O did not change too much when the complex is formed. Almost all the Al-C bond lengths remain unchanged, about 1.97 Å. The O-H bond remains the same when (CH₃)₃Al:OH₂ is formed. The C-Al-C bond angle shrinks from 120° to 118°. This complex is relatively stable comparing with the reactants.

After O₂ molecule is bound with the TMAI-OH₂ complex leading to the formation of TMAI-OH₂:O₂, only a small of energy (0.7kcal/mol) is released. The TMAI-OH₂ molecule was bound with O₂ essentially by hydrogen bond, so the interaction is weak and the geometry of TMAI-OH₂:O₂complex remains almost the same.

After one transition state (^3TS , Figure 3.4.2), this reaction produces $(\text{CH}_3)_2\text{Al}(\text{O}_2)\text{OH}_2$ and one CH_3 radical with 5.1 kcal/mol of endothermicity at the G2M level of theory. The distance between aluminum and O_2 is formed to be significantly decreased when the reaction is completed. The $\text{Al}-\text{O}^a$ bond length is 5.24 Å in the $\text{TMAI}-\text{OH}_2:\text{O}_2$ complex and it decreases to 2.20 Å at the transition state and is finally reduced to 1.93 Å in $(\text{CH}_3)_2\text{Al}(\text{O}_2)\text{OH}_2$. The length of the O_2 double bond is 1.2 Å at the beginning and it is increased to 1.32 Å when the reaction is completed. The energy barrier of the transition state was formed to be 24.2 kcal/mol at the G2M level which indicate that the generation of a reactive product such as radical CH_3 cannot occur readily.



3.5 Associating process of TMAI

Before starting to discuss the reaction between two TMAIs and O_2 , the association process between two TMAI monomers forming a TMAI dimer will be studied first. From a literature review, the association energy between two TMAI monomers has been measured and it is 20.2 kcal/mol[17]. This association energy will be later calculated by different methods. The results from the calculation will be compared with the experimental data to help us choose a reasonable computational method to carry out further study on the whole PES of the reaction between two TMAI monomers and the O_2 molecule.

In fact, the dimerization of TMAI molecules can take place spontaneously. In this step, a large amount of energy is released as alluded to above, suggesting the high stability of the dimer. The structures of monomer-TMAI and dimer-TMAI are shown in Figure 3.5.1., all the geometries were optimized by B3LYP/6-311++G(3df,2p).

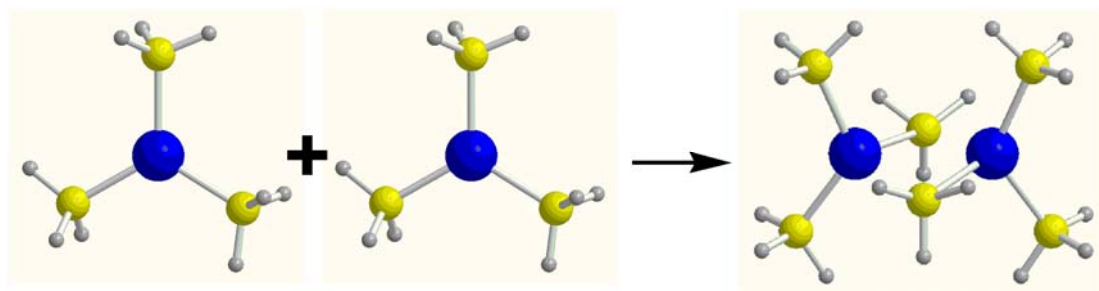


Figure 3.5.1 Association reaction of TMAI

From Figure 3.5.1, the associating process of two TMAI monomers could be observed clearly. They are bound by the interaction between CH₃ and aluminum atoms. One of the carbon atoms in a TMAI monomer binds with another TMAI through the Al atom. This action caused the interacting carbon atoms to stretch slightly from the original Al-C bond length from 1.97 to 2.15 Å. Three of the C-Al-C original angle were 120°, and then changed to 120°, 109° and 105°. Both monomers experienced the same change, in this associating process.

As aforementioned, to choose a reasonable computational method, the experimental association energy is compared with the computational results. as listed in Table 3.5.1.

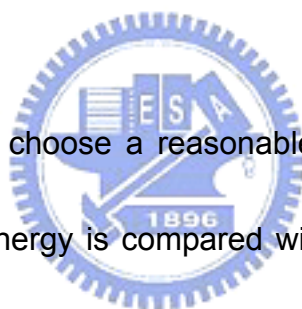


Table 3.5.1 TMAI association energies obtained by different methods

Methods	Association energy
Experiment[17]	-20.20 ± 1 kcal/mol
B3LYP/6-311++G(3df,2p)	-7.56 kcal/mol
G3B3	-21.59 kcal/mol
MP2/6-311++G(d,p)	-18.21 kcal/mol
VASP(PW91)	-16.79 kcal/mol

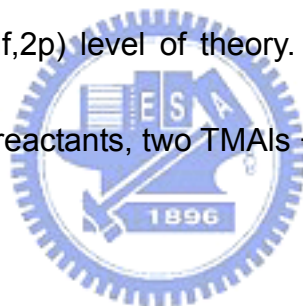
From the experimental work[17], the association energy was determined to

be 20.2 kcal/mole by Laubengayer et al. as given in Table 3.5.3 and also mentioned above. The association energies obtained from the G3B3 and MP2, 21.59 and 18.21 kcal/mol, are the closest values to the experimental data. Accordingly, the G3B3 and MP2 methods were used to carry out the mapping of the whole PES of the reaction of TMAI dimer with O₂. However, due to the size of this system, both of them failed to optimize the entire reaction. Two other computational methods, VASP and B3LYP, were then employed to carry out the calculation for the reaction between two TMAIs and O₂ molecule. The next section (3.6) will focus on discussing the results obtained by B3LYP and VASP only.



3.6 Reaction of two Trimethylaluminums and Oxygen

The geometries of the reactants, intermediates, transition states and products in this reaction were optimized by B3LYP/6-311++G(3df,2p) and the structures are shown in Figure 3.6.1. Details of these geometries are summarized in Table 3.6.1. The atom C^a in Table 3.6.1 represents the methyl which is to be move away from the TMAI molecule. All relative energies of the gas-phase species derived by the calculation are given in Figure 3.6.1. The potential energy diagram shown in Figure 3.6.1 was obtained from calculation at the B3LYP/6-311++G(3df,2p) level of theory. All the relative energies are given with reference to the reactants, two TMAIs + O₂.



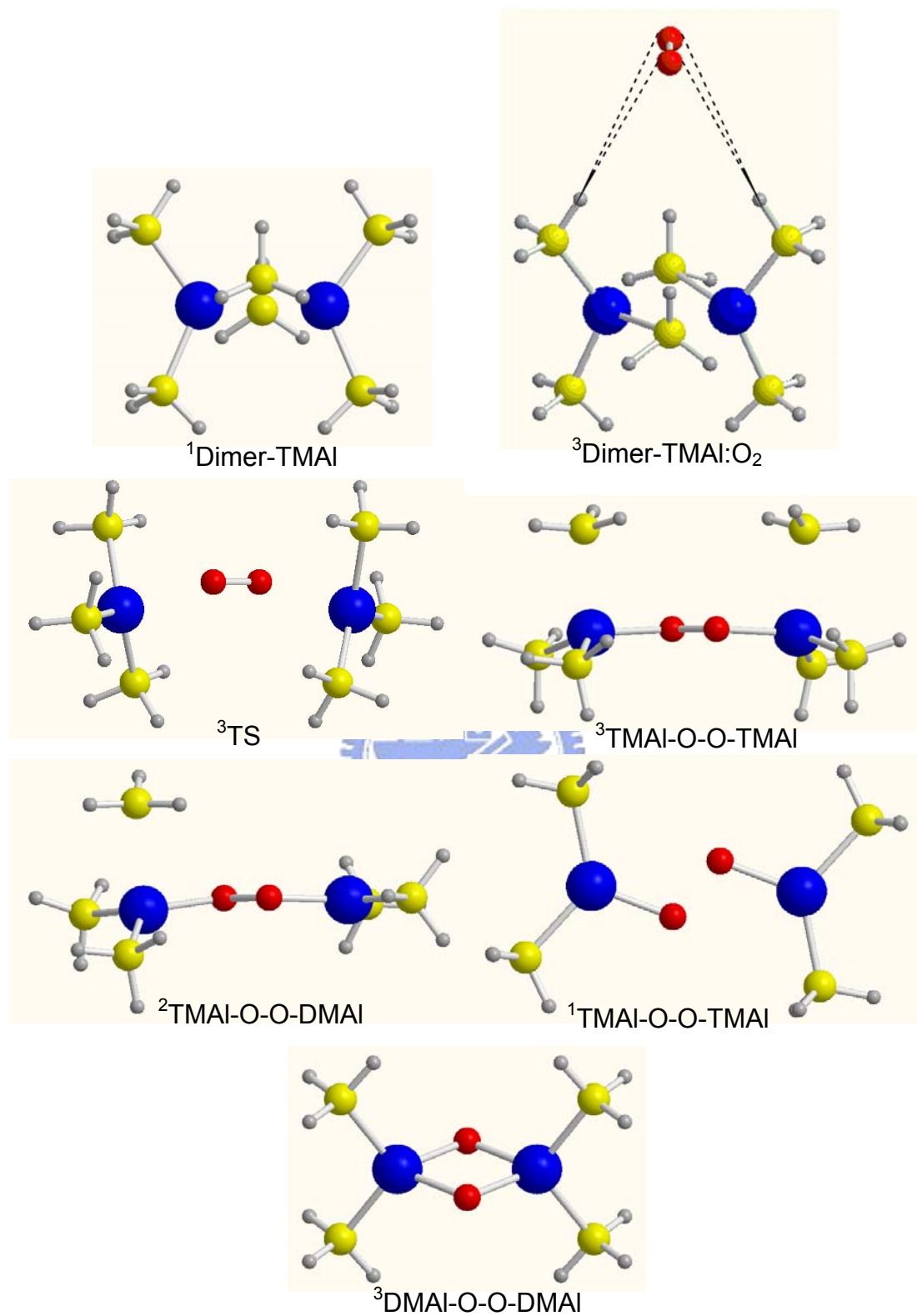


Figure 3.6.1 B3LYP optimized geometries of species involved in reaction



B3LYP 6-311++g(3df,2p)

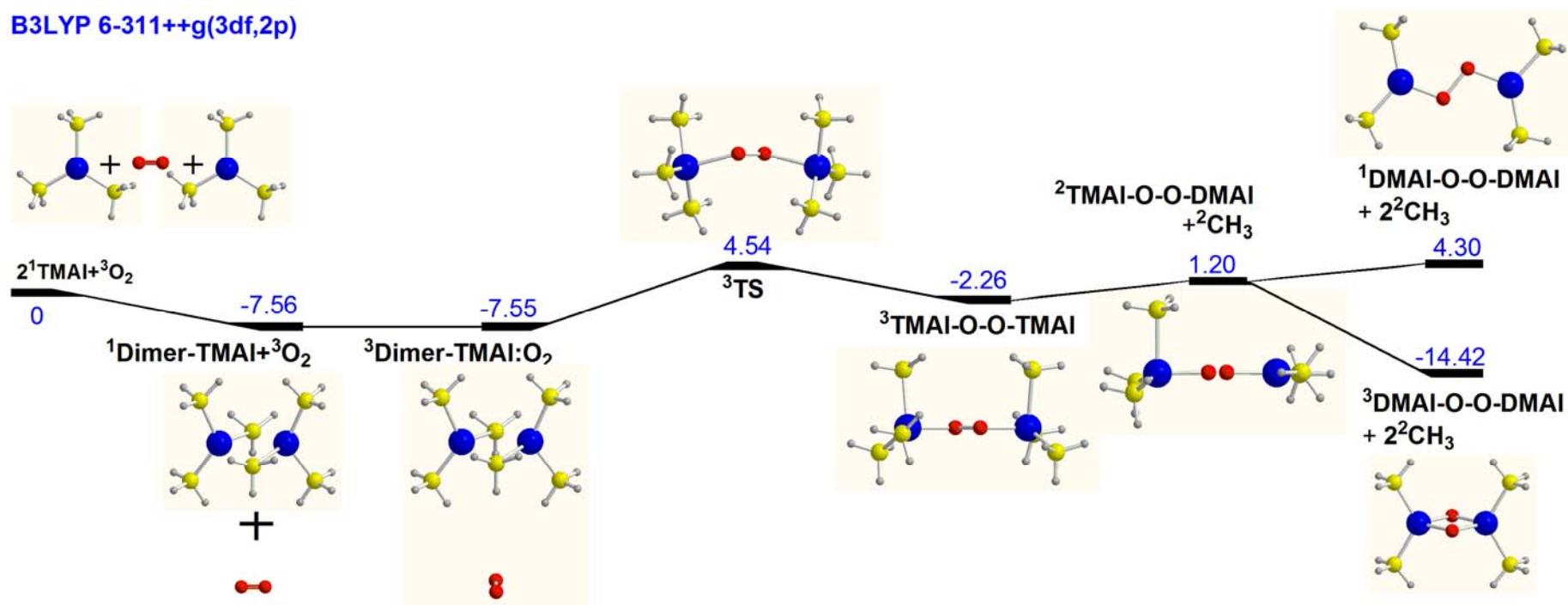


Figure 3.6.2 Potential energy surface of reaction $2TMAI + O_2$ by B3LYP

Table 3.6.1 Geometrical details of species in the dimer-TMAI + O₂ reaction by

B3LYP (Å)

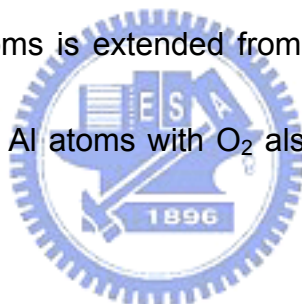
Species	Reactants	¹ Dimer-TMAI+ ³ O ₂	³ Dimer-TMAI:O ₂	TS
R(O-O)	1.20	1.20	1.20	1.24
R(Al-Al)	-	2.62	2.62	4.97
R(Al-O)	-	-	6.11	2.13
R(Al-C)	1.97	1.97	1.97	1.97
R(Al-C ^a)	1.97	2.15	2.15	2.01

Species	³ TMAI-O ₂ -TMAI	² TMAI-O ₂ -DMAI	¹ DMAI-O ₂ -DMAI+CH ₃	³ DMAI-O ₂ -DMAI+2CH ₃
R(O-O)	1.40	1.46	1.47	2.24
R(Al-Al)	4.37	4.24	4.21	2.81
R(Al-O)	1.81	1.77	1.77	1.80
R(Al-C)	1.97	1.97	1.95	2.01
R(Al-C ^a)	2.21	2.32	-	-

As discussed before, two trimethylaluminums exist as a stable dimer which is bridged by two carbon atoms from each of the TMAI. The association energy was predicted to be about 7.56 kcal/mol at B3LYP/6-311++G(3df,2p) level of theory, as shown in the first step in Figure 3.6.2. Although this is different from the experimental result (~20 kcal/mol); they both have the same trend forming a stable complex, dimer-TMAI.

The O₂ molecule is associated bind with the TMAI dimer giving a van der Waals complex, dimer-TMAI:O₂, hence not much energy is released. The geometries of dimer TMAI remain essentially the same before and after its complexation with the O₂ molecule.

After passing through the transition state, the two oxygen atoms directly bond with two TMAl's by attaching with the two Al atoms inside the TMAl to form TMAl-O-O-TMAl. The energy barrier was found to be 4.54 kcal/mol. The reaction can easily overcome the transition state and proceed to give two CH₃ radicals. The O-O bond length was found to increase from 1.20 to 1.40 Å after TMAl-O-O-TMAl was formed as shown in Table 3.6.1, transforming the O=O double bond to a single bond. The participation of O₂ in this reaction caused the TMAl dimer structure to be broken giving TMAl-O-O-TMAl. The distance between two aluminum atoms is extended from 2.62 to 4.37 Å as shown in Table 3.6.1. The binding of Al atoms with O₂ also leads to a decrease in the Al-O bond separation.



The formation of the Al-O bonds also breaks one of the three Al-CH₃ bonds from each TMAl group to give the molecular complex of two CH₃ radicals with the singlet and triplet DMAI-O-O-DMAI as shown in Figure 3.6.2. It should be noted that the energy of triplet DMAI-O-O-DMAI is lower than its singlet analogue according to the B3LYP result. The formation of triplet DMAI-O-O-DMAI is in principle allowed in terms of the overall spin.

We have also scanned the PES with the VASP code. The geometries of the reactants, intermediates, transition states and products are shown in

Figure 3.6.3. The details of these geometries are summarized in Table 3.6.2.

The atom C^a in the Table 3.6.2 represents the methyl which moves away from TMAI. All relative energies of the gas-phase species derived by the calculations are listed in the potential energy diagram in Figure 3.6.4.



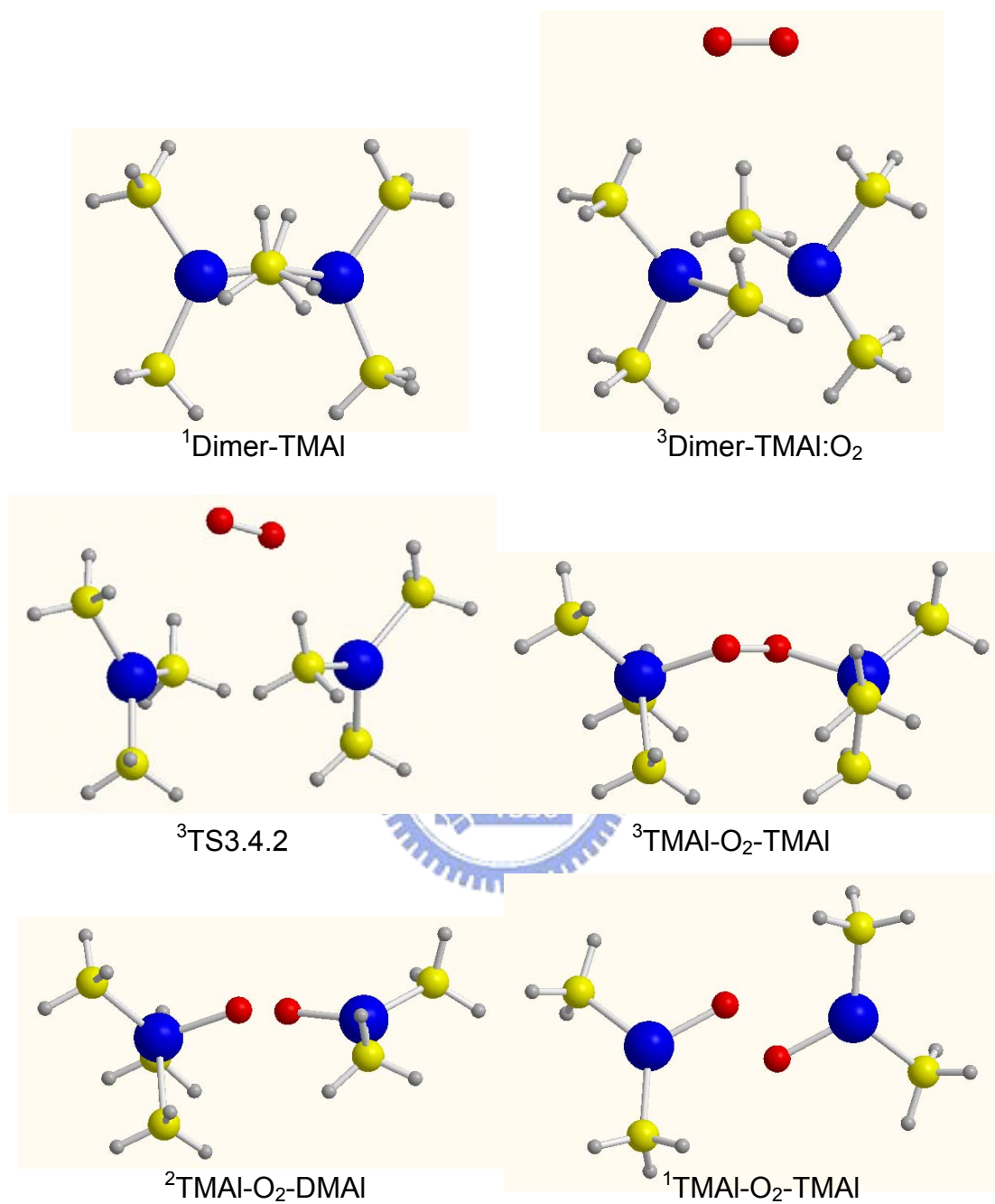


Figure 3.6.3 VASP optimized geometries of species involved in reaction 2TMAI

+ O₂ by VASP

VASP

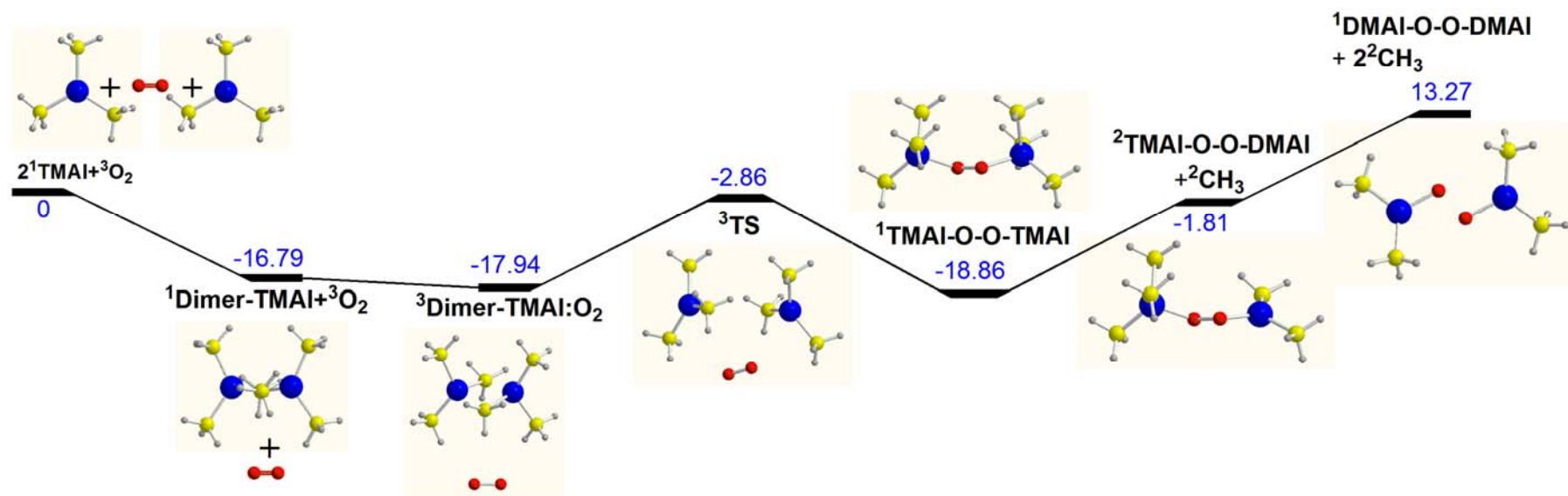


Figure 3.6.4 Potential energy surface of reaction $2\text{TMAI} + \text{O}_2$ by VASP

Table 3.6.2 Geometrical details of species in reaction dimer-TMAI + O₂ by

VASP (Å)

Species	Reactants	¹ Dimer-TMAI+ ³ O ₂	³ Dimer-TMAI:O ₂	TS
R(O-O)	1.24	1.24	1.24	1.24
R(Al-Al)	-	2.62	2.61	4.56
R(Al-O)	-	-	4.60	3.63
R(Al-C)	1.97	1.97	1.97	1.97
R(Al-C ^a)	1.97	2.12	2.15	1.97

Species	³ TMAI-O ₂ -TMAI	² TMAI-O ₂ -DMAI	¹ DMAI-O ₂ -DMAI+CH ₃
R(O-O)	1.36	1.43	1.52
R(Al-Al)	4.35	4.25	4.16
R(Al-O)	1.87	1.77	1.75
R(Al-C)	1.97	1.97	1.95
R(Al-C ^a)	2.08	2.10	-

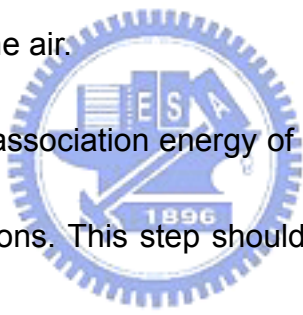
The whole PES carried out by the VASP code is similar to that by B3LYP.

The association energy was found to be 16.79 kcal/mol by VASP, as shown in the first step in Figure 3.6.4. This was much closer to the experimental value (~20 kcal/mol) than that from B3LYP. Computational results from both B3LYP and VASP showed the same trend that two TMAIs produced dimer-TMAI with a reasonable stability.

When the O₂ molecule binds with the TMAI dimer by the van der Waals force, 1 kcal/mol energy is released. The released energy is slightly larger than that calculated by B3LYP. The singlet DMAI-O-O-DMAI, rather than its triplet

analogue, is formed as the final product, after two radicals is expelled. Qualitatively, this is the only different between the result from B3LYP and VASP calculations.

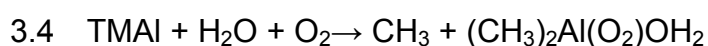
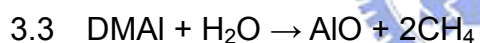
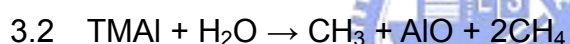
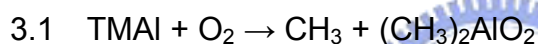
Regardless the spin states of the DMAI- O-O -DMAI product, their energies are not too much different and are not much higher than that of the reactants. Significantly, both the B3LYP and VASP results show that the TMAI dimer reaction with the O₂ molecule has rather low energy barrier and can easily eject two CH₃ radicals in the overall reaction. This result can well explain why TMAI is hypergolic in the air.



In summary, the large association energy of TMAI has been confirmed by quantum chemical calculations. This step should occur spontaneously. In the TMAI dimer + O₂ reaction, two radical CH₃ molecules were predicted to be produced. To produce the radicals, a transition state must be overcome with a small barrier of 4.54 and -2.86 kcal/mol according to the calculations by B3LYP and VASP, respectively. Both values are reasonably small so that the reaction can proceed easily in the air at ambient temperature. The reaction produces two radicals which can energetically react with O₂ to generate more reactive radicals to sustain the combustion of a TMAI gas cloud in the air.

Chapter 4. Conclusion

In this study, the question of “Why is trimethylaluminum (TMAI, $(\text{CH}_3)_3\text{Al}$) hypergolic in the air?” has been investigated quantum mechanically by calculations with the Gaussian code. A series of reactions with high energy released when TMAI contacts with O_2 and H_2O in the air was studied to unveil this hypergolic phenomenon. The following five possible reactions were investigated:



Possible paths of the reactions, and the structures and energetics of the reactants, intermediates, and products were determined by the calculations. In addition, those in the reaction of $2\text{TMAI} + \text{O}_2$ were studied by the VASP calculation as well.

In the reaction of $\text{TMAI} + \text{O}_2$, a stable intermediate could not be formed

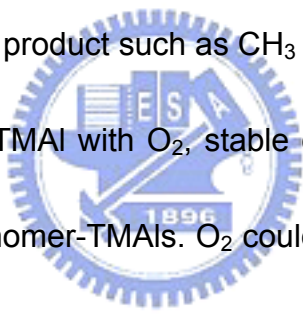
directly. Instead, it takes a place directly via a transition state which lies 17 kcal/mol above the reactants. After the transition state, $(\text{CH}_3)_3\text{AlO}_2$ molecule was formed, in which one of the methyls was slightly pulled away from Al. This methyl could be readily released from Al to give CH_3 with a small amount of activation energy.

In the reaction of $\text{TMAI} + \text{H}_2\text{O}$, TMAI bonds with a water molecule forming a complex, $(\text{CH}_3)_3\text{AlOH}_2$, with 17 kcal/mol energy released. By climbing across a small barrier which was lower than those of the reactants by 0.13 kcal/mol, one methane from the intermediate could be released to form an intermediate, $(\text{CH}_3)_2\text{AlOH}$. It is possible to deliver another methane but it has to overcome an energy barrier of 30 kcal/mol, thus the overall mechanism contains four reactions. The first two reactions are exothermic and can occur readily, whereas the last two processes are endothermic and cannot occur easily at ambient temperature. The barrier for the formation of CH_3AlO is 29.8 kcal/mol which cannot be easily overcome at ambient temperature in the atmosphere.

Another possible path studied involved the reaction of O_2 with dimethylaluminum (DMAI, $(\text{CH}_3)_2\text{Al}$) which was at first formed by dissociating a methyl from TMAI. The reaction of DMAI and water is similar to that of the previous one. The final products are two CH_4 molecules and AlO radical. Their

energy is only 2.5 kcal/mol higher than that of the reactants.

From the computational result of the reaction between TMAI and O₂, TMAI is hard to react directly with the O₂ molecule, so a water molecule was used as a catalyst binding with TMAI in advance. Subsequently, the O₂ molecule is attached to the water complex by van der Waals bonding. The aluminum could be oxidized by the oxygen molecule, releasing one methyl radical from the aluminum via a transition state. The energy barrier of the transition state, however, was found to be 24.2 kcal/mol at the G2M level which indicates that the generation of a reactive product such as CH₃ cannot occur readily.



In the reaction of two TMAI with O₂, stable dimer-TMAI could be formed first by associating two monomer-TMAIs. O₂ could then be bound with a TMAI dimer subsequently by a physical bond. After a relatively low transition state is overcome, TMAI-O₂-TMAI can be readily formed. The intermediate readily releases two methyls with a relatively small barrier, 4.54 and -2.86 kcal/mol computed by B3LYP and VASP, respectively.

In summary, by theoretical simulations, we have elucidated the mechanisms for aforementioned five reactions of TMAI with water and/or oxygen molecules. Among these processes, the reaction of two TMAIs and O₂ can occur with a relatively small barrier; thus it is considered to be the major

pathway to produce CH_3 radicals when TMAI is in contact with air. This result explains why TMAI is hypergolic in the air.



References

1. Zhu, R., C.-C. Hsu, and M.C. Lin, *ab initio study of CH₃+O₂ reaction: kinetics, mechanism and product branching probabilities*. Journal of Chemical Physics, 2001. **115**(1): p. 9.
2. Fock, V., Z. Physik, 1930. **61**: p. 5.
3. Dewar, M.J.S., et al., *Development and use of quantum mechanical molecular models. 76. AM1: a new general purpose quantum mechanical molecular model*. J. Am. Chem. Soc., 1985. **107**(13): p. 8.
4. Stewart, J.J.P., Journal of Computational Chemistry, 1989. **10**.
5. Bacon, A.C. and M.C. Zerner, Theo. Chim. Acta., 1979. **53**.
6. Clementi, E. and D.L. Raimondi, *Atomic Screening Constants from SCF Functions*. Journal of Chemical Physics, 1963. **38**(11): p. 4.
7. Clementi, E., *simple basis set for molecular wavefunctions containing first- and second-row atoms*. Journal of Chemical Physics, 1964. **40**(7): p. 2.
8. Ditchfield, R., W.J. Hehre, and J.A. Pople, *self-consistent molecular-orbital methods. IX. an extended Gaussian-type basis for molecular-orbital of organic molecules*. Journal of Chemical Physics, 1971. **54**(2): p. 5.
9. Collins, J.B., P.v.R. Schleyer, and J.S. Binkley, *self-consistent molecular orbital methods. XVII. geometries and binding energies of second-row molecules. a comparison of three basis sets*. Journal of Chemical Physics, 1976. **64**: p. 10.
10. Clark, T., et al., Journal of Computational Chemistry, 1983. **4**.
11. Hohenberg, P.K. and W. Kohn, Physical review, 1964. **136**.
12. Foresman, J.B., *Exploring Chemistry with Electronic Structure Method. In 2nd ed.*
13. Gonzalez, C. and H.B. Schlegel, *an improved algorithm for reaction path following*. Journal of Chemical Physics, 1989. **90**(4): p. 8.
14. Widjaja, Y. and C.B. Musgrave, *Quantum chemical study of the mechanism of aluminum oxide atomic layer deposition*. Applied Physics Letters, 2002. **80**(18): p. 3304-3306.
15. Ghosh, M.K. and C.H. Choi, *The initial mechanisms of Al₂O₃ atomic layer deposition on OH/Si(100)-2 x 1 surface by tri-methylaluminum and water*. Chemical Physics Letters, 2006. **426**(4-6): p. 365-369.
16. Raghunath, P. and M.C. Lin, *Computational study on the mechanisms and energetics of trimethylindium reactions with H₂O and H₂S*. Journal of Physical Chemistry A, 2007. **111**(28): p. 6481-6488.

17. Laubengayer, A.W. and W.F. Gilliam, *The Alkyls of the Third Group Elements. I. Vapor Phase Studies of the Alkyls of Aluminum, Gallium and Indium*. *Journal of the American Chemical Society*, 1941. **63**: p. 477-479.

